

## H $\alpha$ Variability of AB Aur b with the Hubble Space Telescope: Probing the Nature of a Protoplanet Candidate with Accretion Light Echoes

BRENDAN P. BOWLER,<sup>1,2</sup> YIFAN ZHOU,<sup>3</sup> LAUREN I. BIDDLE,<sup>2</sup> LILLIAN YUSHU JIANG,<sup>2</sup> JAEHAN BAE,<sup>4</sup> LAIRD M. CLOSE,<sup>5</sup>  
KATHERINE B. FOLLETTE,<sup>6</sup> KYLE FRANSON,<sup>2,\*</sup> ADAM L. KRAUS,<sup>2</sup> ANIKET SANGHI,<sup>7,†</sup> QUANG TRAN,<sup>8,‡</sup>  
KIMBERLY WARD-DUONG,<sup>9</sup> YA-LIN WU,<sup>10</sup> AND ZHAOHUAN ZHU<sup>11</sup>

<sup>1</sup>*Department of Physics, University of California, Santa Barbara, Santa Barbara, CA 93106, USA*

<sup>2</sup>*Department of Astronomy, The University of Texas at Austin, Austin, TX 78712, USA*

<sup>3</sup>*Department of Astronomy, University of Virginia, 530 McCormick Rd, Charlottesville, VA 22904, USA*

<sup>4</sup>*Department of Astronomy, University of Florida, Gainesville, FL 32611, USA*

<sup>5</sup>*Department of Astronomy, University of Arizona, 933 N. Cherry Ave., Tucson, AZ 85718, USA*

<sup>6</sup>*Amherst College, Department of Physics and Astronomy, USA*

<sup>7</sup>*Cahill Center for Astronomy and Astrophysics, California Institute of Technology, 1200 E. California Boulevard, MC 249-17, Pasadena, CA 91125, USA*

<sup>8</sup>*Department of Astronomy, Yale University, New Haven, CT 06511, USA*

<sup>9</sup>*Five College Astronomy Department, Amherst College, Amherst, MA 01002, USA*

<sup>10</sup>*Department of Physics, National Taiwan Normal University, Taipei 116, Taiwan*

<sup>11</sup>*Department of Physics and Astronomy, University of Nevada, Las Vegas, 4505 South Maryland Parkway, Las Vegas, NV 89154-4002, USA*

### ABSTRACT

Giant planets generate accretion luminosity as they form. Much of this energy is radiated in strong H $\alpha$  line emission, which has motivated direct imaging surveys at optical wavelengths to search for accreting protoplanets. However, compact disk structures can mimic accreting planets by scattering emission from the host star. This can complicate the interpretation of H $\alpha$  point sources, especially if the host star itself is accreting. We describe an approach to distinguish accreting protoplanets from scattered-light disk features using “accretion light echoes.” This method relies on variable H $\alpha$  emission from a stochastically accreting host star to search for a delayed brightness correlation with a candidate protoplanet. We apply this method to the candidate protoplanet AB Aur b with a dedicated Hubble Space Telescope Wide Field Camera 3 program designed to sequentially sample the host star and the candidate planet in H $\alpha$  while accounting for the light travel time delay and orbital geometry of the source within the protoplanetary disk. Across five epochs spanning 14 months, AB Aur b is over 20 times more variable than its host star; AB Aur’s H $\alpha$  emission changes by 15% while AB Aur b varies by 330%. These brightness changes are not correlated, which rules out unobstructed scattered starlight from the host star as the only source of AB Aur b’s H $\alpha$  emission and is consistent with tracing emission from an independently accreting protoplanet, inner disk shadowing effects, or a physically evolving compact disk structure. More broadly, accretion light echoes offer a novel tool to explore the nature of protoplanet candidates with well-timed observations of the host star prior to deep imaging in H $\alpha$ .

*Keywords:* planets and satellites: formation — planets and satellites: individual (AB Aurigae)

Corresponding author: Brendan P. Bowler  
bpbowler@astro.as.utexas.edu

\* NSF Graduate Research Fellow

† NSF Graduate Research Fellow.

‡ 51 Pegasi b Fellow

### 1. INTRODUCTION

Giant planets assemble the vast majority of their mass by accreting material from circumplanetary disks nested within more massive gas-rich protoplanetary disks. This process of giant planet growth is not well understood

compared to accretion in the stellar regime, where infalling gas is heated as it accelerates along magnetic field lines and collides with the protostar to produce shocks and hot spots (e.g., Hartmann et al. 2016). Together these give rise to hot continuum emission in the UV, veiling across the optical spectrum, and strong, broad, emission lines (e.g., Herbig 1962, Calvet & Gullbring 1998; Ingleby et al. 2013).

In the planetary regime, the geometry of accretion is still an open question and likely depends on the planetary magnetic field strength and properties of the circumplanetary disk. For example, gas accretion may proceed through spherically symmetric flows, predominantly at the poles, or through magnetospheric accretion columns (Zhu 2015; Aoyama et al. 2018; Thanathibodee et al. 2019; Marleau et al. 2022). However, even the basic elements underpinning these models are largely unconstrained by observations including the characteristic timescale and location of giant planet formation; the behavior of planetary accretion rate histories (e.g., steady-state or episodic; Fortney et al. 2008; Dong et al. 2021); circumplanetary disk masses, temperatures, and geometries (Ward & Canup 2010; Lubow & Martin 2012; Zhu et al. 2016); and the mechanism of mass and angular momentum transfer from the protoplanetary disk through the circumplanetary disk and onto the young planet (Bryan et al. 2018; Batygin 2018; Bryan et al. 2020). Finding and confirming young accreting protoplanets is the first step to begin to address these questions.

Directly detecting UV continuum emission from young planets requires space-based observations (e.g., Zhou et al. 2021), but optically bright hydrogen recombination lines—most notably  $H\alpha$ —offer a convenient approach to search for accreting planets. However, high-contrast imaging in  $H\alpha$  has been difficult because of technical challenges and conflicting interpretations of results. Ground-based adaptive optics (AO) systems are traditionally optimized for infrared wavelengths, so specialized instruments are needed to achieve high Strehl ratios in the visible (e.g., MagAO, Close et al. 2014; MagAO-X, Males et al. 2020; SCEXAO/VAMPIRES, Norris et al. 2015; SPHERE/ZIMPOL, Schmid et al. 2018; VLT/MUSE, Bacon et al. 2010). This has enabled the first generation of high-contrast imaging surveys targeting young stars in  $H\alpha$  (e.g., Cugno et al. 2019; Zurlo et al. 2020; Xie et al. 2020; Huélamo et al. 2022; Follette et al. 2023; Cugno et al. 2023). Some space-based imaging in  $H\alpha$  has been carried out with the Hubble Space Telescope, but its modest angular resolution and lack of advanced coronagraphic capabilities for starlight suppression have limited surveys to modest sample sizes

(e.g., Zhou et al. 2014; Sanghi et al. 2022; Zhou et al. 2022).

Although several accreting protoplanet candidates were identified in these campaigns, many of these detections and their interpretations have been contested. LkCa 15 is a prominent example; multiple point sources were identified in thermal emission and  $H\alpha$  (Kraus & Ireland 2012; Sallum et al. 2015a), but their nature has been called into question because of confusion with inner disk structures (e.g., Thalmann et al. 2016; Currie et al. 2019; Blakely et al. 2022). Compact features from an inner disk may be mimicking planets by preferentially scattering light from the host star. These bright regions can appear point-like and result in false positive planet signals (Follette et al. 2017; Rameau et al. 2017). Sallum et al. (2023) found that the LkCa 15 inner disk substructure is variable and may be tied to physical evolution of these features on timescales of months to years, illustrating the challenges involved in validating young planet candidates.

The clearest case of accreting protoplanets is in the PDS 70 system, which harbors two directly imaged planets nested within a large transition disk gap (Keppler et al. 2018; Müller et al. 2018; Haffert et al. 2019). Both planets were found to be accreting through deep  $H\alpha$  imaging (Wagner et al. 2018; Haffert et al. 2019; Hashimoto et al. 2020; Zhou et al. 2021; Close et al. 2025; Zhou et al. 2025, in press), and circumplanetary dust has been detected around PDS 70 c with ALMA (Isella et al. 2019; Benisty et al. 2021). This system has provided the clearest window into the planet assembly process and the properties of their circumplanetary disks.

Recently, a concentrated feature was detected within the protoplanetary disk surrounding AB Aurigae (AB Aur; Currie et al. 2022; Zhou et al. 2022), a young ( $\approx 2$ – $4$  Myr), intermediate-mass ( $\approx 2.4 M_{\odot}$ ) accreting A0 star in the greater Taurus-Auriga complex (DeWarf et al. 2003). AB Aur and its large complex disk have been well-studied for many decades (e.g., Sanford & Merrill 1958; Marsh et al. 1995; Mannings & Sargent 1997; Betti et al. 2022). Millimeter observations show a large dust cavity out to about 120 AU with two spiral structures detected within the dust ring (Tang et al. 2017; Jorquera et al. 2022). A central compact radio-bright source has been found to be consistent with an outflow from AB Aur (Rodríguez et al. 2014; Rivière-Marichalar et al. 2023; Rota et al. 2024). Grady et al. (1999) identified regular sporadic infall of material onto AB Aur which may be related to evaporating exocomets, and infrared variability of the disk itself has been observed over a broad range of timescales and wavelengths (Shenavrin

et al. 2019; Prusti & Mitsukevich 1994; Chen & Jura 2003). On larger scales, outer spiral arms extend to at least  $\sim 450$  AU (Grady et al. 1999; Fukagawa et al. 2004; Corder et al. 2005; Perrin et al. 2009). Speedie et al. (2024) recently found evidence of gravitational instability from kinematic signatures in ALMA isovelocity maps, suggesting that the disk may be susceptible to gravitational collapse.

There have been hints of planets within the AB Aur disk in several datasets (e.g., Oppenheimer et al. 2008; Boccaletti et al. 2020), including the faint source (“AB Aur b”) identified by Currie et al. (2022) at a projected separation of  $\approx 0''.6$  ( $\approx 90$  AU). Currie et al. (2022) recovered AB Aur b in multiple epochs from the ground and archival Hubble Space Telescope (HST) observations spanning the optical to near-infrared. They argued that the resolved nature of the source, the lack of a detection in polarized light, signs of orbital motion, and the spatial location coincident with the trailing edge of an inner spiral arm all point to an embedded giant planet.

Zhou et al. (2022) identified the source in H $\alpha$  as part of a high-contrast imaging survey of transition disk hosts with HST’s Wide Field Camera 3 (WFC3). They found elevated emission but note that the H $\alpha$  line-to-continuum ratio is similar to that of the host star, raising the possibility that AB Aur b is a compact disk structure and the H $\alpha$  line emission is reflected light from the accreting host star. Moreover, strong scattered light features are prevalent throughout the disk including in the vicinity of AB Aur b. In a follow-up study, Zhou et al. (2023) recovered AB Aur b in the UV and blue optical with HST and confirmed that its short-wavelength spectral energy distribution (SED) is dominated by scattered stellar light based on a strong Balmer break, which would not be expected for a planet but is in good agreement with reflected light from the A0 host star. Despite this progress, the true nature AB Aur b remains elusive and more observational tests are needed to distinguish between a disk structure or an embedded accreting protoplanet.

Here, we present a new method to test whether an H $\alpha$  point source is an accreting planet or a compact disk feature seen in scattered light. This strategy relies on “accretion light echoes” caused by variable accretion onto the host star to probe the nature of the companion. In combination with other lines of evidence, this technique can be used distinguish accreting planets like those orbiting PDS 70 from false positive signals caused by disk substructure, as appears to be the case with LkCa 15. We apply this technique to the recently identified candidate protoplanet AB Aur b with a dedicated

narrow-band H $\alpha$  imaging program using HST/WFC3, in which carefully timed sampling of the host star is carried out prior to deep observations of the companion across five epochs to establish whether stochastic accretion from the host star is also witnessed in variability of the companion.

This study is organized as follows. In Section 2 we describe the geometric setup of the accretion light echo problem and discuss measurements that are needed to determine the orbital orientation of the planet candidate. We present the HST observations of AB Aur in Section 3 and results of the accretion light echo experiment for AB Aur b in Section 4. Potential interpretations of the variability results are discussed in Section 5. A summary of results can be found in Section 6.

## 2. ACCRETION LIGHT ECHOES AS A TEST OF THE PROTOPLANET HYPOTHESIS

Light echoes have long been used as a tracer of dust structure in the vicinity of time-variable sources. Applications include the identification of historic supernovae (Rest et al. 2012), probing AGN accretion disks via reverberation mapping (Bahcall et al. 1972; Blandford & McKee 1982), resolving structure in protoplanetary disks (Gaidos 1994; Ortiz et al. 2010), and even searching for planetary companions (Argyle 1974; Bromley 1992; Sparks et al. 2018; Bromley et al. 2021). This technique relies on variable emission from a central source and subsequent delayed scattering of that signal, usually from nearby circumstellar or interstellar dust. Because scattering from a compact disk feature can mimic an accreting protoplanet, this method can naturally be used to test the nature of H $\alpha$  point sources around young stars such as AB Aur in the absence of other sources of variability.

### 2.1. Geometry of Accretion Light Echoes

The travel time for a pulse of light originating from the host star to a source at an orbital distance  $r$  is  $r/c$ . The time delay ( $\Delta t$ ) for a distant observer to see the same signal scattered from the orbiting body depends on the orbital geometry and its position in its orbit relative to the observer’s line of sight. This orientation can be characterized by  $\omega + \nu(t)$ , where  $\omega$  is argument of periastron—the angle between the longitude of ascending node and periastron passage—and the true anomaly  $\nu$ —the time-dependent angle between periastron and the position of the orbiting body. When the planet is on the near side of its orbit closest to Earth,  $\omega + \nu(t)$  spans  $0-\pi$ , and on the far side of the orbit  $\omega + \nu(t)$  spans  $\pi-2\pi$ .

In the context of using an accretion light echo to probe the nature of a directly imaged H $\alpha$  source, the goal is to

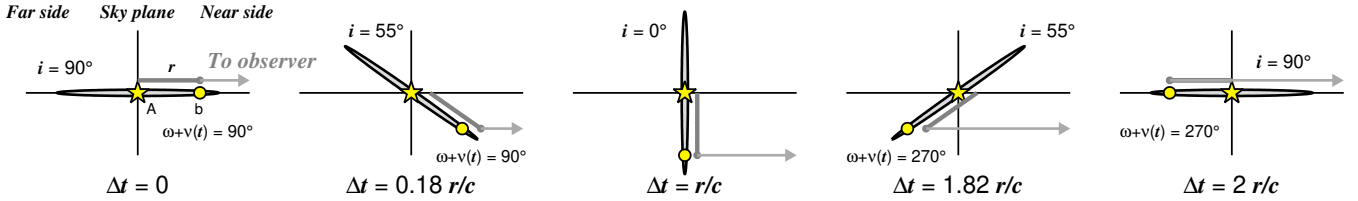


**Figure 1.** Examples of the impact of orbital geometry on light echo time delays. Stochastic changes in the brightness of a host star (from episodic accretion, for instance) will be seen as delayed variability from a compact disk feature at an orbital distance  $r$ . This time delay will range from 0 at inferior conjunction ( $\omega + \nu(t) = \pi/2$ ; left panel) to  $r/c$  in the sky plane (middle panel) to  $2r/c$  at superior conjunction ( $\omega + \nu(t) = 3\pi/2$ ; right panel).

test whether the source is reflecting light from the host star or whether its brightness variations are behaving independently. In the former case, any variable emission (e.g., H $\alpha$  line strength) from the companion would be caused by earlier stochastic changes in the accretion rate onto the host star. Here, the orbit of the H $\alpha$  source can be assumed to lie within the plane of a protoplanetary disk. Figure 1 illustrates some simple examples for varying disk inclinations. For an edge-on disk, a dust clump located at inferior conjunction (on the front side of the disk closest to the observer where  $\omega + \nu(t) = \pi/2$ ), there is no lag between emission from the host star and scattered light so  $\Delta t = 0$ . At superior conjunction (on the far side of the disk where  $\omega + \nu(t) = 3\pi/2$ ), the distance traveled is twice the orbital radius and the maximum delay time is  $\Delta t = 2r/c$ . Positions in the plane of the sky produce a delay of  $\Delta t = r/c$ , which occur for a face-on orientation, for the quadrature points of a circular orbit, or more generally when  $\omega + \nu(t)$  is equal to 0 or  $\pi$ . For context, this characteristic timescale  $r/c$  is 42 min at 5 AU and 13.9 hr for a distant companion at 100 AU. All other orbital geometries will fall between these extremes (0–2  $r/c$ ) and will depend on the orbital inclination  $i$  with respect to the plane of the sky and orbital phase in the following way:

$$\Delta t = \frac{r}{c} \left( 1 - \sin(i) \sin(\omega + \nu(t)) \right). \quad (1)$$

The first term ( $r/c$ ) is the time it takes for light to travel from the host star to the companion at a distance  $r$ , and the second term is the time to traverse the component of the companion’s position along the line of sight orthogonal to the sky plane. The difference is the extra time (and distance) to reach the observer after the scattering event. This relationship assumes a circular orbit but can readily be extended to elliptical orbits with a time-dependent orbital distance (e.g., Sparks et al. 2018). Figure 2 illustrates this time lag as a function of orbital phase for various orbital inclinations.

## 2.2. Application to AB Aurigae

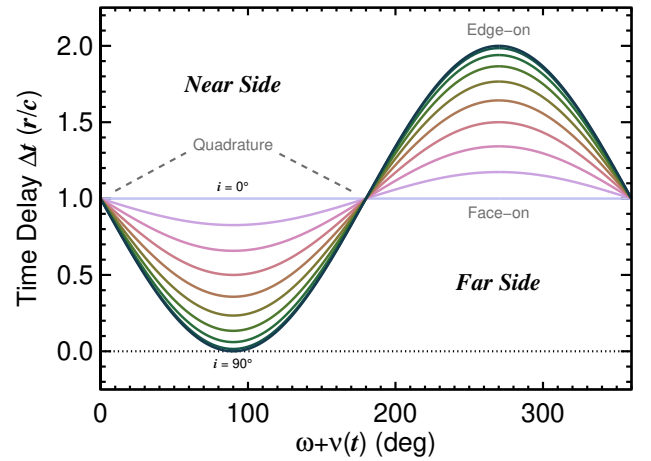


**Figure 2.** Time delay of light echoes as a function of orbital phase ( $\omega + \nu(t)$ ). Time delays are shown in units of  $r/c$ , which is the time it takes for light to travel from the star to the companion. Inclinations from  $0^\circ$  to  $90^\circ$  are shown in steps of  $10^\circ$ . Depending on the inclination and location in the orbit, the time delay can reach a minimum of 0 and a maximum of  $2r/c$ , depending on the three-dimensional geometry of the system. For the application to accreting protoplanets, this highlights the need to determine the disk inclination, the disk orientation, and the current position of the companion in its orbit to accurately compute the expected time delay for a light echo.

This method of accretion light echoes requires that the host star be sufficiently variable, either in continuum or line emission (such as H $\alpha$  or Pa $\beta$ ). Moreover, if the rate of stochastic brightness variations is slow—for instance, days or weeks—compared to the light travel time of the orbiting companion, then the impact of the time delay will not be important. In this case simultaneous observations of the host and companion would be sufficient for this experiment. On the other hand, if episodic accretion is fast—on timescales of minutes or hours—then the time delay should properly be taken into account, and separate observations are needed for the host and then again later for the companion. The variability proper-



ties of the host star are therefore relevant for the design of an accretion light echo experiment.

AB Aur is actively accreting at a rate of  $\approx 10^{-7} M_{\odot} \text{ yr}^{-1}$  (Salyk et al. 2014) and shows strong changes in the H $\alpha$  emission line profile and overall strength at the level of tens of percent on a variety of timescales ranging from hours to years (e.g., Herbig 1960; Finkenzeller 1983; Catala et al. 1999; Harrington & Kuhn 2007; Costigan et al. 2014). Moreover, the H $\alpha$  emission line intensity is much greater than the continuum level: Harrington & Kuhn (2007) find typical peak line intensities about 10 times higher than the continuum emission. Changes in the H $\alpha$  emission line strength are therefore expected to dominate the overall variability at this wavelength.

Accretion also produces significant broadband variability. AB Aur shows brightness changes at the level of 0.1 mag in optical light curves from the Microvariability and Oscillations of Stars (MOST) satellite spanning 24 days in 2009 and 2010 (Cody et al. 2013). More recently, AB Aur was monitored in six 27-day sectors from December 2019 to December 2024 by the Transiting Exoplanet Survey Satellite (TESS; Ricker et al. 2014); details of the TESS light curve extraction and analysis are discussed in Section 3.1. The TESS lightcurves show short-term brightness changes at the few-percent level over day-to-week timescales (Figure 3). Interestingly, the behavior of AB Aur in the latest TESS lightcurve (Sector 86 in December 2024) shows sharp 3% variations that fall and rise on day-long timescales, which bear some resemblance to dipper stars (albeit with lower amplitudes) and could be a sign that close-in occulting circumstellar disk material is contributing to the optical variations (e.g., Capistrant et al. 2022). Altogether the combination of rapid accretion-induced broadband and H $\alpha$  variability make AB Aur an excellent testbed for carrying out an accretion light echo experiment with the wide candidate protoplanet AB Aur b.

For most applications of accretion light echoes, the orbit of the source of interest may not be well constrained if it was recently discovered or if the candidate is located at a wide separation with a correspondingly long orbital period. Moreover, even with full coverage of the orbital period, an orbit based on relative astrometry alone is not enough to distinguish the full three-dimensional geometry of the orbital plane because there exists a 180° degeneracy in the longitude of ascending node. This is the case for AB Aur b, which orbits due south of its host star at a projected separation of 0''.6, or 93 AU. If AB Aur b is on the near side of the sky plane, the light echo time delay will be less than  $r/c$ , but if it is on the far side, the lag time greater than  $r/c$ . There are ways

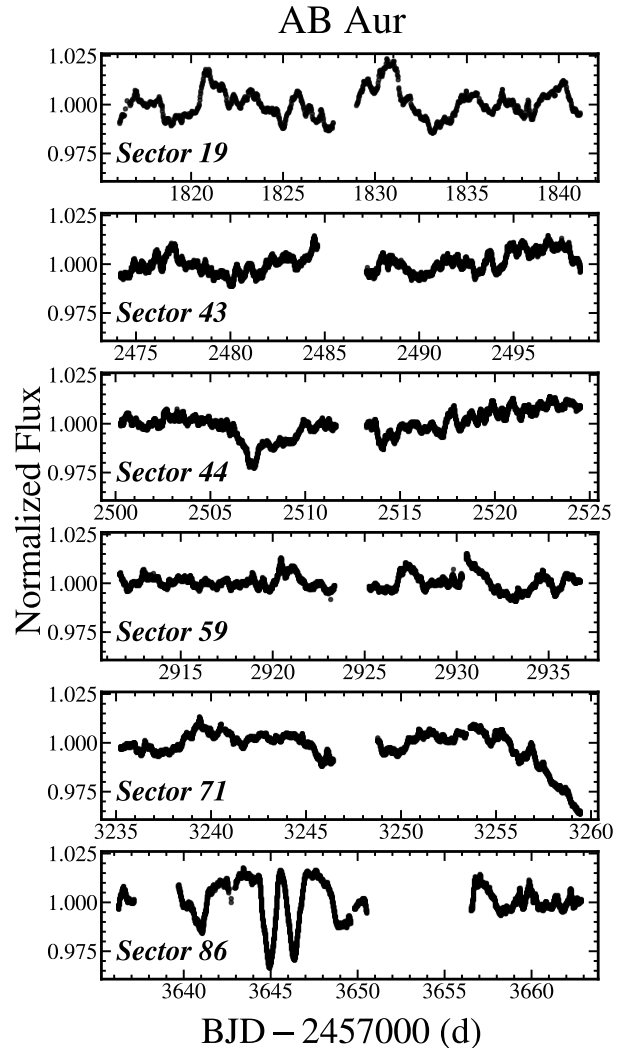


**Figure 3.** Normalized TESS light curves of AB Aur from Sectors 19, 43, 44, 59, 71, and 86. The variability within each Sector of a few percent suggests only modest changes in accretion rate over month-long baselines.

to break this degeneracy using disk kinematics or spiral arm morphology, as discussed below.

Currie et al. (2022) detected orbital motion in the counterclockwise direction based on over a decade of astrometric measurements.<sup>1</sup> Information about the geometric orientation of the orbit can be obtained from spatially resolved mm imaging of the disk to yield its inclination and probe its velocity structure. Together

<sup>1</sup> Additional epochs obtained with HST by Zhou et al. (2022) and Zhou et al. (2023) do not appear to follow the same clear trend. This could be caused by instrument-to-instrument systematics or perhaps alternative approaches to modeling the position of the source given its resolved nature. Nevertheless, for this study we treat counterclockwise motion as a true indication of the orbital direction of AB Aur b.

this is enough to break the degeneracy in the longitude of ascending node and determine if the southern side of the inclined disk is closer to Earth than the northern side, or vice versa.

There is a long history of spatially resolved mapping of AB Aur’s dust and gas disk spanning the near-infrared to cm wavelengths. Although the physical properties of the disk have been studied in depth, the large size and complex morphology of the disk have at times yielded disk parameters that disagree in their details. Below we summarize recent observational constraints on the inclination and geometric orientation of AB Aur’s disk, which we then use to determine the expected delay time for an accretion light echo experiment.

Scattered-light  $H$ -band imaging from Fukagawa et al. (2004) yielded  $i_d = 30 \pm 5^\circ$  and a P.A. of  $58 \pm 5^\circ$  for the orientation of the major axis of the disk. Similarly, Perrin et al. (2009) found a range of  $22\text{--}35^\circ$  for the disk inclination from HST/NICMOS scattered-light polarized and total-intensity observations, and Hashimoto et al. (2011) determined an inclination of  $27\text{--}43^\circ$ .

Resolved millimeter studies offer an alternative approach to measuring the disk orientation, rotation axis, and gas kinematics. At a scale of  $\sim 100$  AU, Rivière-Marichalar et al. (2020) found an inclination of  $\approx 24.9^\circ$  and a P.A. of the disk axis of  $\approx -37^\circ$  based on 1.3 mm NOEMA interferometric observations. Tang et al. (2017) reported high-resolution ( $0''.1$ ) ALMA 1.3 mm continuum and CO line observations of the dust ring and inner CO spiral structure. They found a disk inclination of  $23^\circ$  and a P.A. of  $-36^\circ$  for the disk rotation axis. More recently, Speedie et al. (2024) observed AB Aur with ALMA in Band 6 and found a P.A. of  $236.7 \pm 0.3^\circ$  (measured east of north to the redshifted major axis) from fitting the  $C^{18}O$  moment1 map and adopting a disk inclination of  $23^\circ$ .

Complex structure has been observed in the AB Aur disk at larger spatial scales of several hundred AU. Corder et al. (2005) observed AB Aur at  $2''$  resolution in  $^{13}CO$ ,  $^{18}CO$ ,  $^{12}CO$ , and 2.7 mm continuum emission with the Owens Valley Radio Observatory millimeter-wave array. They found a disk inclination of  $21.5^{+0.4}_{-0.3}$  and PA of  $58.6 \pm 0.5^\circ$ . Piétu et al. (2005) targeted AB Aur with the IRAM Plateau de Bure interferometer in CO and mm continuum intensity emission. They measured inclinations of  $\approx 33^\circ$  to  $42^\circ$  and PAs of  $-27^\circ$  to  $-31^\circ$ , but they note that these values may be impacted by unresolved structure and asymmetric emission. Piétu et al. conclude that an inclination of  $\approx 23^\circ$  is most likely as it reconciles the measured velocities and the expected mass of AB Aur. Tang et al. (2012) confirm an incon-

sistency of the inclination measured on different spatial scales—from  $\approx 42^\circ$  at large scales to  $\approx 23^\circ$  at the location of the dust ring at  $\approx 100\text{--}200$  AU—which could be explained by a warp in the disk.

We adopt a disk inclination of  $23 \pm 2^\circ$  and PA of the disk rotation axis of  $-36 \pm 5^\circ$  based largely on observations from Rivière-Marichalar et al. (2020) and Tang et al. (2017), which probed spatial scales similar to AB Aur b. Here the uncertainties have been estimated to encapsulate the most precise measurements. The rotation axis PA implies a PA for the longitude of ascending node,  $\Omega$ , of  $54 \pm 5^\circ$  assuming AB Aur b is nested in the disk<sup>2</sup>. The northeastern side of the disk is blueshifted and the southwestern side is redshifted (e.g., Corder et al. 2005; Tang et al. 2012; Tang et al. 2017; Speedie et al. 2024); combined with the counterclockwise orbital motion of AB Aur b from Currie et al. (2022), this implies the brighter southeast portion of the disk is on the near side and the northwest portion of the disk is on the far side. AB Aur b therefore appears to be on the near side of the disk. As noted by Fukagawa et al. (2004), this geometry is reinforced by the larger-scale spiral structure of the disk, which would be trailing in this configuration.

Finally, the orbital distance of AB Aur b,  $r$ , can be determined from the projected separation  $\rho$  and its orbital phase using the Thiele-Innes elements. Assuming a circular orbit, and converting the argument of periastron and true anomaly ( $\omega + \nu(t)$ ) to measured angles of the disk and companion ( $\Delta PA$ ), the de-projected orbital semi-major axis is

$$r = \frac{\rho}{\varpi \sqrt{\cos^2(\Delta PA) + \cos^2(i) \sin^2(\Delta PA)}} \text{ AU}, \quad (2)$$

where  $\rho$  is the projected separation in units of  $''$ ,  $\varpi$  is the system parallax in  $''$ ;  $\Delta PA$  (equal to  $|PA - \Omega|$ ) is the difference between the position angle of the companion (measured East of North), PA, and the longitude of ascending node,  $\Omega$ ; and  $i$  is the orbital (and, equivalently, the disk) inclination. Here  $r$  is expressed in units of AU.

Using the parallax to AB Aur from Gaia DR3 ( $\varpi = 6.4127 \pm 0.0372$  mas; Gaia Collaboration et al. 2016; Gaia Collaboration et al. 2022), the mean projected separation of  $574 \pm 15$  mas from Zhou et al. (2023), the companion PA of  $181.2 \pm 2.1$  from Zhou et al. (2023), and  $\Omega$  and  $i$  from our adopted values for the disk, we find a true separation of  $r = 94 \pm 5$  AU for AB Aur

<sup>2</sup> This assumption of coplanarity with the disk is reinforced by AB Aur b’s resolved nature, possibly associated with a circumplanetary disk or envelope, and connections to larger scale features in the disk (e.g., Currie et al. 2022; Zhou et al. 2022).

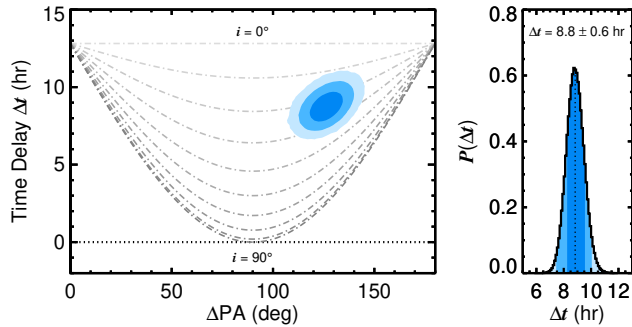


**Figure 4.** Predicted delay time,  $\Delta t$ , for light echoes from AB Aur b. Inclinations from  $0^\circ$  to  $90^\circ$  are shown in steps of  $10^\circ$ . Left: The protoplanetary disk inclination ( $23 \pm 2^\circ$ ), orientation of the disk’s rotation axis ( $-36 \pm 5^\circ$ ), and position of AB Aur b in its orbit correspond to a constraint in the expected delay time. These are represented here with 1-, 2-, and 3- $\sigma$  contours in joint constraints of  $\Delta t$  as a function of  $\Delta\text{PA}$ , the absolute difference between the companion PA and the longitude of ascending node. Right: Marginalized distribution delay times for AB Aur b. Our best estimate is  $\Delta t = 8.8 \pm 0.6$  hr.

b. This corresponds to a characteristic light travel time of  $r/c = 13.1 \pm 0.75$  hr to reach AB Aur b, and a *delay* time of  $\Delta t = 8.8 \pm 0.6$  hr based on Monte Carlo realizations of  $\Delta\text{PA}$  and  $i$  (Figure 4).

Here we have only considered the disk midplane where a planet would reside. If the disk is flared, this will have a modest influence on the predicted arrival time of scattered light off of small grains in the disk atmosphere. For AB Aur b, the impact would effectively be a higher inclination angle and a somewhat smaller delay time compared to the geometrically flat disk we have assumed. See Gaidos (1994) for details of light echoes for a flared disk.

### 3. OBSERVATIONS

#### 3.1. TESS Light Curves of AB Aur

AB Aur was observed by TESS in Sectors 19, 43, 44, 59, 71, and 86. We downloaded the light curves of each sector from the Mikulski Archive for Space Telescopes (MAST) data archive. For Sector 19, only full-frame image (FFI) light curves are available (Caldwell et al. 2020b). For Sectors 43, 44, 59, 71, and 86 we used the *lightkurve* (Lightkurve Collaboration et al. 2018) software package to obtain the 2-minute cadence TESS light curve (Smith et al. 2012; Stumpe et al. 2012; Stumpe

et al. 2014; Jenkins et al. 2016).<sup>3</sup> All photometry listed as NaN are first removed. Then, light curves from all sectors are stitched together and median normalized by dividing the flux and flux errors by the median flux of the combined light curve.

#### 3.2. Hubble Space Telescope WFC3/UVIS Imaging

Deep H $\alpha$  imaging of AB Aur was carried out with HST (GO 17168; PI: Bowler) across five epochs spanning 20 orbits from January 2023 to March 2024 (UT 2023 January 7–8, 2023 February 7–8, 2023 March 1–2, 2024 February 21–22, March 4–5) using WFC3’s ultra-violet and visible light (UVIS) channel and the *F656N* narrow-band filter ( $\lambda_c = 6561.4$  Å;  $\Delta\lambda = 17.6$  Å)<sup>4</sup> Each epoch consists of four orbits; the first orbit is designed to measure the H $\alpha$  flux emitted from the host star followed by a second visit of three contiguous orbits at a later time to sample AB Aur b. These three orbits during the second visit are required to reach a sufficient total exposure time and depth to recover AB Aur b in a similar fashion as in Zhou et al. (2022). Observations for other HST programs are taken in between these visits.

The spacing of the first and second visits is intended to capture the time delay associated with light traveling from the host star to AB Aur b and scattering to an observer, which depends on the physical separation of the companion and its orbital geometry as described in Section 2.2. HST’s orbital period is about 96 min, with typical blocks of about 50 min available for guide-star acquisition and science observations. This means the “effective time resolution” of each 3-orbit set of observations focused on AB Aur b from the beginning of Orbit 2 to the end of Orbit 4 for each epoch is about 242 min ( $96 \text{ min} \times 2 + 50 \text{ min}$ ), or roughly 4 hours, with the midpoint occurring about 2 hours into the sequence. The expected time delay for the light echo from AB Aur b to an observer is about 9 hours (Figure 4). Given the uncertainties in the geometry of the system, the start of the observations are within 2–3  $\sigma$  of the predicted timing of the light echo for each of the five epochs.<sup>5</sup> The gap in time between the first (Orbit 1) and second (Orbits 2–4) visits from this program was about 10 hours (for epochs E1–E4) and 12 hours for one

<sup>3</sup> TESS FFI and 2-minute cadence light curves are available at MAST: Caldwell et al. (2020a) and MAST Team (2021) respectively.

<sup>4</sup> The data is available at MAST: <http://dx.doi.org/10.17909/cve2-6v41>.

<sup>5</sup> If the inclination is larger than expected, this will reduce the time delay and increase the tension between the predicted time and the observation start time. For instance, a  $42^\circ$  inclination gives a predicted delay time of 6.0 hours.

**Table 1.** HST WFC3/UVIS Imaging of AB Aur in F656N

Orbit	Obs. Epoch	UT Date	Mean Julian Date <sup>a</sup>	$\Delta t$ <sup>b</sup>	Exp. Time	$N_{\text{Dith.}} \times N_{\text{Exp.}}$	HST Roll Angle <sup>c</sup>	Notes <sup>d</sup>
Epoch ID	(UT)	(Y-M-D)	(JD - 2457000)	(hr)	(s)		( $^{\circ}$ )	
E1	2023.0190	2023-01-07	2952.43701	0.0	2.7	4 × 11	80.0	AB Aur A
E1	2023.0203	2023-01-08	2952.89964	11.10	2.7	4 × 11	112.0	AB Aur b
E1	2023.0205	2023-01-08	2952.96572	12.69	2.7	4 × 11	80.0	AB Aur b
E1	2023.0206	2023-01-08	2953.03181	14.28	2.7	4 × 11	112.0	AB Aur b
E2	2023.1040	2023-02-07	2983.44316	0.0	2.7	4 × 11	76.0	AB Aur A
E2	2023.1052	2023-02-08	2983.90499	11.08	2.7	4 × 11	103.5	AB Aur b
E2	2023.1054	2023-02-08	2983.97107	12.67	2.7	4 × 11	76.0	AB Aur b
E2	2023.1056	2023-02-08	2984.03715	14.26	2.7	4 × 11	103.5	AB Aur b
E3	2023.1639	2023-03-01	3005.31240	0.0	2.7	4 × 11	70.0	AB Aur A
E3	2023.1651	2023-03-02	3005.77483	11.10	2.7	4 × 11	95.0	AB Aur b
E3	2023.1653	2023-03-02	3005.84089	12.68	2.7	4 × 11	70.0	AB Aur b
E3	2023.1655	2023-03-02	3005.90695	14.27	2.7	4 × 11	95.0	AB Aur b
E4	2024.1406	2024-02-21	3361.97654	0.0	2.7	4 × 11	78.2	AB Aur A
E4	2024.1419	2024-02-21	3362.43782	11.07	2.7	4 × 11	103.2	AB Aur b
E4	2024.1421	2024-02-22	3362.50372	12.65	2.7	4 × 11	78.2	AB Aur b
E4	2024.1423	2024-02-22	3362.56961	14.23	2.7	4 × 11	103.2	AB Aur b
E5 <sup>e</sup>	2024.1749	2024-03-04	3374.49667	0.0	2.7	4 × 11	63.2	AB Aur A
E5	2024.1763	2024-03-05	3375.02381	12.65	2.7	4 × 11	88.2	AB Aur b
E5	2024.1765	2024-03-05	3375.08969	14.23	2.7	4 × 11	63.2	AB Aur b
E5	2024.1767	2024-03-05	3375.15558	15.81	2.7	4 × 11	88.2	AB Aur b

<sup>a</sup>Average JD of the start of the first science observation and the end of the last observation for each orbit.

<sup>b</sup>Elapsed time since first orbit in each four-orbit sequence.

<sup>c</sup>Position angles are in HST’s V3 coordinate system.

<sup>d</sup>Notes about the intended science goals of each orbit. Although all orbits have the same setup, the first orbit in each epoch is designed to sample the host star flux, then after a gap in time, Orbits 2-4 are taken back-to-back to recover the candidate protoplanet AB Aur b.

<sup>e</sup>For Orbit 1 of epoch E5, the Fine Guidance Sensors did not acquire the guide stars until after the observations were complete so guiding was carried out with GYRO pointing control. However, this did not significantly impact the quality of the observations nor the results from this epoch.

epoch (E5), corresponding to a wait time of 6–7 orbits. This is slightly longer than the expected time delay by about 1–3 hours from the end of Orbit 1 to the start of Orbit 2, or 3.5–5.5 hours from the midpoint of Orbit 1 to the midpoint of Orbit 3. Nevertheless, this modest “overshooting” is an improvement over a scenario with no gap in the four orbit scheduling of each epoch, which would have resulted in an underestimate of 6.5 hours, or in which the host star flux was directly obtained from the 3 orbits dedicated for the companion, which would have underestimated the time delay by 9 hours.

Special scheduling constraints are imposed to avoid diffraction spikes from AB Aur falling at the position of the companion, located at a separation of  $0''.6$  from the host star. Each 4-orbit group is taken with relative roll angle requirements between 25–35 $^{\circ}$  in an A-BAB

pattern (representing Orbit 1 followed by Orbits 2–4 at a later time) to facilitate PSF subtraction through angular differential imaging (ADI; Liu 2004; Marois et al. 2006). Here “A” refers to one roll angle orientation and “B” refers to the second roll angle. Actual roll angles range from 25–32 $^{\circ}$  among the five epochs. Images are taken with the UVIS2-C512C-SUB 512×512 pix subarray, resulting in a field of view of  $20''.5 \times 20''.5$  for the WFC3/UVIS plate scale of 40 mas pix $^{-1}$ . The same setup is used for all four orbits of each epoch.

A WFC3-UVIS-DITHER-BOX 4-point dither pattern is employed with  $0''.02$  spacing between positions for cosmic ray rejection and to mitigate bad pixels. For each dither pointing, 11 images in *F656N* are acquired, each with an exposure time of 2.7 s, resulting in 880 frames altogether and a total on-source integration time of 2376 s



**Table 2.** F656N Photometry and Astrometry of AB Aur b

Epoch	Epoch	Host Count Rate <sup>b</sup>	Host $f_\nu$ <sup>b</sup>	AB Aur b Count Rate <sup>c</sup>	AB Aur b $f_\nu$ <sup>c</sup>	P.A.	$\rho$	$\sigma_x$ <sup>d</sup>	$\sigma_y$ <sup>d</sup>
ID	(UT)	(e <sup>-</sup> s <sup>-1</sup> )	(mJy)	(e <sup>-</sup> s <sup>-1</sup> )	(mJy)	( $^\circ$ )	( $''$ )	( $''$ )	( $''$ )
E0 <sup>a</sup>	2022.17	440829 $\pm$ 6900	10540 $\pm$ 170	96 $\pm$ 11	2.29 $\pm$ 0.26	182.3 $\pm$ 1.1	0.595 $\pm$ 0.009	0.086	0.062
E1	2023.020	357720 $\pm$ 229	8554 $\pm$ 5	180 $\pm$ 9	4.30 $\pm$ 0.22	182.3 $\pm$ 1.0	0.594 $\pm$ 0.007	0.11	0.071
E2	2023.105	363580 $\pm$ 610	8694 $\pm$ 15	65 $\pm$ 9	1.55 $\pm$ 0.21	178.3 $\pm$ 1.2	0.582 $\pm$ 0.008	0.092	0.054
E3	2023.165	331200 $\pm$ 730	7920 $\pm$ 17	64 $\pm$ 6	1.52 $\pm$ 0.15	180.0 $\pm$ 1.0	0.583 $\pm$ 0.008	0.085	0.058
E4	2024.142	373650 $\pm$ 380	8935 $\pm$ 9	272 $\pm$ 18	6.50 $\pm$ 0.43	181.7 $\pm$ 1.0	0.591 $\pm$ 0.008	0.11	0.082
E5	2024.176	324590 $\pm$ 550	7762 $\pm$ 13	148 $\pm$ 10	3.53 $\pm$ 0.23	184.4 $\pm$ 1.0	0.594 $\pm$ 0.007	0.094	0.057

<sup>a</sup> “E0” is a new reduction of HST WFC3/UVIS H $\alpha$  observations from Zhou et al. (2022). These data did not include a delayed sampling of the host star, AB Aur, and the candidate companion AB Aur b.

<sup>b</sup> Measured from Orbit 1 of each epoch, with the exception of E0.

<sup>c</sup> Measured from Orbits 2–4 of each epoch, with the exception of E0.

<sup>d</sup> Standard deviations of the best-fitting 2-D Gaussian model used in forward modeling. These represent widths of the input model, not the deconvolved implied angular size of AB Aur b.

(40 min). However, as the first orbit of each epoch is intended to sample the host star’s H $\alpha$  emission, only 132 frames are used for the reduced image of AB Aur b, amounting to an exposure time of 356 s (5.9 min) at each epoch. A minimum of 10 days between epochs is imposed to ensure AB Aur’s H $\alpha$  variability is sampled on timescales that are uncorrelated with the previous epoch. The first three epochs were taken within a three month period in early 2023, and the last two epochs were obtained in early 2024. The corresponding epoch-to-epoch baselines range from 12 days to nearly one year. Details of the observations can be found in Table 1.

In addition to new observations taken as part of this accretion light echo program, we also uniformly re-reduce previously obtained H $\alpha$  observations of AB Aur taken with WFC3/UVIS in F656N (GO 16651; PI: Zhou). These data were presented in Zhou et al. (2022) and span five orbits across two visits separated by nearly two months: three orbits on UT 2022 February 7 and two orbits on UT 2022 March 28. Although this dataset did not include a light travel time delay between the host and candidate companion as in this survey, the observations were otherwise carried out in a similar fashion and offer an opportunity to analyze longer-term variability about 10 months prior to the first epoch from this program. We refer to this epoch from 2022.17 as Epoch 0 (“E0”) and the five epochs from this survey spanning 2023.02 to 2024.176 as Epochs 1–5 (“E1” to “E5”).

### 3.3. WFC3 Data Reduction

The data processing largely follows procedures described in Zhou et al. (2022) and Zhou et al. (2023). The reduction starts with the f1c FITS files downloaded

from the MAST archive. These files are processed by the `calwf3` pipeline, which includes calibrations of bias, flat field, and charge transfer efficiency corrections. Cosmic rays and bad pixels are identified from the calibrated images and replaced by bilinear interpolation of neighboring pixels. A small number of bad pixels persist throughout each epoch and are flagged using Data Quality (DQ) values 1024 (charge trap sink pixels) and 4096 (cosmic rays detected by `AstroDrizzle`), with remaining spurious pixels identified by eye in epoch-averaged images. We find that this approach is more robust than using DQ flags alone. There are no bad pixels apparent near the companion. Images are registered and assembled into data cubes by aligning the centroid positions of AB Aur to a common origin through sub-pixel image resampling. The native plate scale of 40 mas pixel<sup>-1</sup> is preserved throughout the image processing and analysis.

Photometry of the host star is measured for every image taken within the first of four orbits of each epoch using aperture photometry with a radius of 10 pixels (0 $''$ .4). A correction is then applied for UVIS2 encircled energy loss with the F656N filter<sup>6</sup>. Count rates are converted to flux densities using the inverse sensitivity conversion factors contained in the `PHOTFLAM` FITS header keyword. Average count rates and flux densities of AB Aur are presented in Table 2. Intra-orbit and inter-orbit light curves are further discussed in Appendix A.

PSF subtraction is carried out using the Karhunen-Loève Image Projection (KLIP; Soummer et al. 2012)

<sup>6</sup> <https://www.stsci.edu/hst/instrumentation/wfc3/data-analysis/photometric-calibration/uvis-encircled-energy>

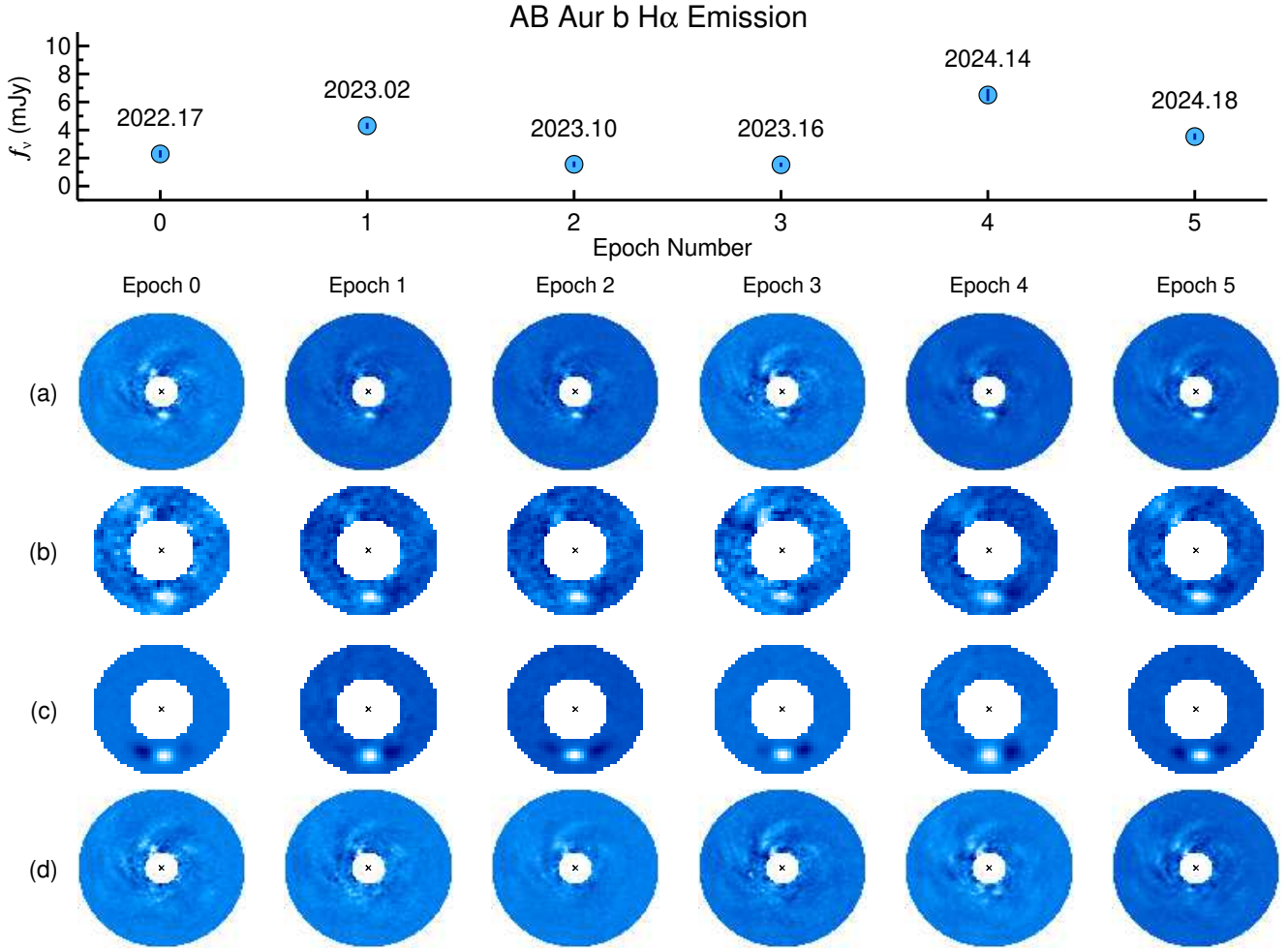


**Figure 5.** HST/WFC3-UVIS H $\alpha$  ( $F656N$  filter) observations of the candidate protoplanet AB Aur b. Epochs E1–E5 originate from our accretion light echo experiment, which spans a 14-month time baseline in 2023–2024, while epoch E0 (originally presented in Zhou et al. 2022) was acquired in 2022 and has been reprocessed here in the same way as the new epochs. *Upper panel:* H $\alpha$  flux density in mJy as a function of epoch number. AB Aur b shows strong variability at the  $14.7\sigma$  level, with brightness increasing by 330% from E3 to E4; see Section 4.1 for details. *Panel (a):* Primary-subtracted images of AB Aur for epochs E0–E5. AB Aur b as well as fainter disk features are clearly visible in each frame. Orbits 2, 3, and 4 are used for frames E1–E5, while E0 represents all five orbits from that program (GO-16651). *Panel (b):* Zoom-in on AB Aur b, located  $0''.6$  south of the host star. The dark lobes on either side of the source are artifacts caused by self-subtraction of AB Aur b using frames acquired at different roll angles. *Panel (c):* Best-fit 2D Gaussian model of AB Aur b from the forward-modeling procedure described in Section 3.4. AB Aur b is resolved, with greater extended emission in the azimuthal direction. *Panel (d):* Residuals after subtracting the best-fit model in Panel (c). North is up and East is to the left in all images. For scale, the inner radius is  $0''.4$  (62 AU) and the outer annulus in Panels (a) and (d) is  $2''.0$  (312 AU).

algorithm implemented with the pyKLIP package (Wang et al. 2015). Following Zhou et al. (2023), each science frame makes use of reference images of all other observations with a minimum roll angle difference of  $20^\circ$ . The number of KL modes is set to 30 for all reductions. KLIP is applied in seven annuli spanning  $0''.1$  to  $2''.0$ . After PSF subtraction, each frame is north aligned, then all observations from Orbits 2–4 of each epoch are coadded into a single processed image.

### 3.4. Astrometry and Photometry

AB Aur b is clearly recovered in the primary-subtracted frames for all five epochs (Figure 5). The morphology of the source appears similar to its appearance in primary-subtracted HST images from Zhou et al. (2023) spanning the UV through optical wavelengths. AB Aur b is the brightest source in the processed frames and is clearly extended in the azimuthal (East-West) direction.

To account for self-subtraction from the ADI processing, photometry and astrometry are measured in `pyKLIP` by forward modeling a 2D Gaussian assuming independence of the  $x$  and  $y$  spatial directions (that is, no covariance is included). The Gaussian standard deviations ( $\sigma_x$  and  $\sigma_y$ ) are determined from direct fits to the primary-subtracted image. Then, three-parameter posteriors are sampled with Markov-chain Monte Carlo: the central position of the source and the amplitude. Uniform priors are adopted for each parameter, and the median and standard deviation of the posterior chains are adopted for the reported central values and corresponding uncertainties. Results are listed in Table 2, and the best-fitting models and residuals of the fits for each epoch are shown in Figure 5.

The inferred position angle ranges from  $178.3^\circ$  (E2) to  $184.4^\circ$  (E5), and the separation is about  $0''.6$  in all epochs. These are in good agreement with previous measurements in Currie et al. (2022), Zhou et al. (2022), and Zhou et al. (2023). The dispersion in the azimuthal direction is consistently larger than that in the radial direction, with an average value of  $\sigma_x = 0''.096$ , which subtends an angle of  $9^\circ$  at separation of  $0''.6$  from the host star, and an average of  $\sigma_y = 0''.064$  in the radial direction. The resulting aspect ratio is  $\sigma_x/\sigma_y = 1.5$ . For comparison, the HST diffraction limit at H $\alpha$  is 29 mas (FWHM = 68 mas); AB Aur b is therefore spatially resolved in both directions. The deconvolved size of AB Aur b is 91 mas and 57 mas in the azimuthal and radial directions, respectively, corresponding to a physical size of 14 AU  $\times$  9 AU at the distance of AB Aur. This is larger than the upper limits of  $\sim 1$ –5 AU for the other spatially unresolved circumplanetary disks surrounding PDS 70 c and SR 12 c (Benisty et al. 2021; Wu et al. 2022). Because the source is spatially resolved, the positional uncertainty of AB Aur b is likely to be underestimated when considering only the spread in the posterior distributions of the  $x$  and  $y$  position from the forward modeling process. We therefore include an additional spread of 10% of the average of  $\sigma_x$  and  $\sigma_y$  in quadrature with the inferred positional uncertainty of AB Aur b as a conservative estimate of potential systematic errors in astrometry. This 10% value represents the approximate scale of the difference in dispersion estimates from the individual reduced frames. These inflated errors are included in the astrometric measurements listed in Table 2.

Note that the recovered astrometry and photometry of AB Aur b as part of our newly reduced E0 epoch differs slightly from—but is formally consistent with—measurements of the same dataset from Zhou et al. (2022). Here we find a separation of  $595 \pm 9$  mas and

a P.A. of  $182^\circ 3 \pm 1'.1$ , which is in good agreement with the separation of  $600 \pm 22$  mas and P.A. of  $182^\circ 5 \pm 1'.4$  from Zhou et al. (2022). On the other hand, we recover slightly higher value for the brightness of AB Aur b; we measure a flux density of  $2.29 \pm 0.26$  mJy, compared with  $1.5 \pm 0.4$  mJy from Zhou et al. (2022). Although our value is 53% larger, given the uncertainties, the two measurements are nevertheless consistent at the  $1.7\sigma$  level. The difference can be attributed to the point-source model used in Zhou et al. (2022) compared with the more accurate extended source model that we adopt here.

## 4. RESULTS

### 4.1. Strong H $\alpha$ Variability from AB Aur b

One simple approach to assess variability of brightness measurements is to compare the characteristic uncertainty of individual measurements,  $\sigma_{\bar{f}_\nu}$ , to the sample standard deviation,  $s = \sqrt{1/(N-1) \cdot \sum_{i=1}^N (f_{\nu,i} - \bar{f}_\nu)^2}$ , where  $N$  is the number of data points,  $f_{\nu,i}$  is the  $i$ th brightness measurement, and  $\bar{f}_\nu$  is the sample mean. A ratio  $\sigma_{\bar{f}_\nu}/s$  near unity would be expected for data without significant variability, whereas a ratio  $\ll 1$  points to real changes. For the five epochs spanning 14 months sampled with this HST program,  $\sigma_{\bar{f}_\nu}/s = 0.11$ . Including E0, this ratio is  $0.12^7$ . AB Aur b shows clear epoch-to-epoch brightness changes that are a factor of 8–10 higher than would be expected from measurement scatter alone.

We can further quantify the significance of variability by computing the  $\chi^2$  value of a constant model assuming no variability as the null hypothesis and comparing this to the expected range of  $\chi^2$  values for the appropriate degrees of freedom,  $\nu$ . Considering all six epochs, we find a  $\chi^2$  value of 235 for  $\nu = N-1 = 5$ , where  $\chi^2 = \sum_{i=1}^N (f_{\nu,i} - c_\nu)^2 / \sigma_{f_{\nu,i}}^2$ . Here  $c_\nu$  is the optimally scaled constant model which minimizes  $\chi^2$  and can be found analytically for model values  $m_{\nu,i}$ :  $c_\nu = \sum_{i=1}^N (f_{\nu,i} m_{\nu,i} / \sigma_{f_{\nu,i}}^2) / \sum_{i=1}^N (m_{\nu,i}^2 / \sigma_{f_{\nu,i}}^2)$  (Cushing et al. 2008). When  $m_{\nu,i}$  is an arbitrary constant, for instance 1, then the scale factor is  $c_\nu = \sum_{i=1}^N (f_{\nu,i} / \sigma_{f_{\nu,i}}^2) / \sum_{i=1}^N (1 / \sigma_{f_{\nu,i}}^2)$ , which is the weighted mean of flux density measurements. For AB Aur b,  $c_\nu$  is 2.58 mJy.

The SNR in effective standard deviations of a Gaussian distribution is  $n = \sqrt{2} \operatorname{erf}^{-1}(\int_0^{\chi^2} \chi'^2 (x|\nu = 5) dx)$ ,

<sup>7</sup> Note that this analysis does not account for slight reddening to AB Aur, which was estimated by McJunkin et al. (2014) to be  $A_V = 0.51$  mag. Extinction to AB Aur b could be significantly greater if it is indeed an embedded protoplanet.

where  $\chi^2(x|\nu = 5)$  is the probability density function of the chi-square distribution for 5 degrees of freedom<sup>8</sup>. For a  $\chi^2$  value of 235, this constant-brightness model can be ruled out in favor of real variability at the  $14.7\sigma$  level. Although we have no reason to believe our photometric uncertainties are underestimated, *if* the errors were to be inflated by a factor of 2, the constant model would result in a  $\chi^2$  value of 58.9 and would still be strongly disfavored at the  $6.7\sigma$  level.

The two faintest epochs are E2 and E3, which were taken within one month of each other from February to March 2023 and have similar flux densities of  $1.55 \pm 0.21$  mJy and  $1.52 \pm 0.15$  mJy, respectively. The brightest epoch is E4 with a flux density of  $6.50 \pm 0.43$  mJy, taken in February 2024. This represents an overall brightening by a factor of 4—specifically, a  $330 \pm 50\%$  increase from its faintest state—over a time baseline of about one year between the observations. The re-reduction of the E0 dataset from 2022 (ten months prior to E1) yields a flux density that is overall comparable to the range that is seen from 2023–2024.

Variations over much shorter timescales are also observed across the coarse sampling of this program. AB Aur b dimmed by 64% from  $4.30 \pm 0.22$  mJy to  $1.55 \pm 0.21$  mJy over a one month period between epochs E1 and E2. It similarly dimmed by 46% from  $6.50 \pm 0.43$  mJy to  $3.53 \pm 0.23$  mJy from E4 to E5 over 13 days.

#### 4.2. Modest $H\alpha$ Variability from AB Aur

The host star AB Aur also shows clear signs of  $H\alpha$  variability in the HST dataset. Here we first consider variability within the first orbit for epochs E1–E5, and similarly for the first of the five orbits for E0. Overall the brightness changes *within* each  $\approx 50$ -min epoch are small. For E1–E5, AB Aur is variable at the sub-percent level with an average standard deviation of 0.14%. This suggests that appreciable changes in mass accretion are occurring on longer timescales. E0 consists of 5 orbits across two visits over two months; the host star flux density in Table 2 is the mean over all five orbits and the quoted relative uncertainty is 1.6%—an order of magnitude larger than for the other epochs, likely a result of the time gap between Orbits 1–3 and Orbits 4–5 for that epoch.

On the other hand, AB Aur shows more substantial epoch-to-epoch variability. The overall scatter is 11.4% for E0–E5, and 6.1% for E1–E5. AB Aur experiences

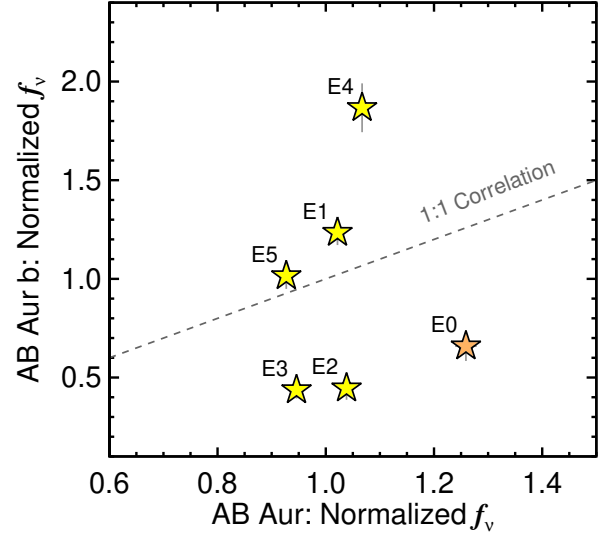


**Figure 6.** Comparison between normalized HST  $H\alpha$  photometry of AB Aur and delayed brightness measurements of the candidate protoplanet AB Aur b (yellow stars). If AB Aur b is an unobscured static disk feature, a positive linear correlation would be expected between AB Aur and AB Aur b. Instead, in this accretion light echo experiment we find that AB Aur varies by about 15% while AB Aur b varies by 330% (epochs E1–E5). For comparison, our new reduction of the HST “E0” epoch from Zhou et al. (2022) is displayed with an orange star. Note, however, that this dataset does not include the time delay between the host and candidate accreting planet. All measurements have been normalized to the mean values of the host star and companion from epochs E1–E5.

a brightness change by a factor of 1.15, or 15%, from minimum (E5) to maximum (E0). This is similar to the expected level of  $H\alpha$  variability based on previous spectroscopic monitoring campaigns (e.g., Harrington & Kuhn 2007; Costigan et al. 2014), and is comparable to the 15% change measured by Zhou et al. (2022) over the course of about two months. It is also comparable to the continuum variability seen in the TESS light curves, which are taken before E0 (Sectors 19, 43, and 44), between E0 and E1 (Sector 59), between E3 and E4 (Sector 71), and after E4 (Sector 86). The uncertainty-to-scatter ratio,  $\sigma_{f_\nu}/s$ , is 0.015 across all six epochs and 0.03 for E1–E5, a sign that the observed scatter exceeds measurement uncertainties by a factor of 30–70. Following the same framework from Section 4.1 to assess the significance level of the observed variability, we find a  $\chi^2$  value of 6947 for a constant-flux model, which corresponds to a  $\sim 80\sigma$  detection of variability for  $\nu=5$  degrees of freedom. This does not seem to be driven by E0, which is the most discrepant epoch; excluding E0 gives  $\chi^2=6800$  ( $\nu=4$ ) with a comparable SNR.

<sup>8</sup> For a Gaussian distribution, the probability that a value falls within  $\pm n$  standard deviations from the mean is  $\text{erf}(n/\sqrt{2})$ , where  $\text{erf}$  is the error function defined as  $\text{erf}(z) \equiv 2/\sqrt{\pi} \int_0^z e^{-t^2} dt$ .



#### 4.3. AB Aur and AB Aur b have Uncorrelated Variability

AB Aur b is clearly much more variable than the host star: AB Aur exhibited  $15.1 \pm 0.2\%$  brightness changes throughout this program while AB Aur b experienced changes at the  $330 \pm 50\%$  level—a factor of  $22 \pm 3$  higher than the host. This alone is a strong sign that emission from these two objects is unrelated. Despite the inconsistent amplitudes, is this variability of the host star correlated with that of AB Aur b? Figure 6 compares the normalized photometry of the host and companion for all five epochs of this accretion light echo experiment. If AB Aur b is a static scattered-light disk feature, an approximately linear correlation would be expected because changes in host star accretion would be directly and proportionately mimicked in the delayed images of AB Aur b. This is not what is observed; epochs E1–E5 significantly depart from a 1:1 correlation by 21% for E1, 57% for E2, 54% for E3, 75% for E4, and 9% for E5. Furthermore, there is no evident pattern in the variations; E2 and E3 are fainter than the 1:1 trend line, while E1, E4, and E5 are brighter. We conclude that the H $\alpha$  emission from AB Aur b cannot *only* be unobstructed scattered light from the host star.

For comparison, we also include the location of E0 in Figure 6, although we emphasize that those observations were not taken as part of this accretion light echo experiment, and when comparing the host brightness to that of the companion, cannot be evaluated in the same self-consistent manner. Nevertheless, we note that for E0, the host star was appreciably brighter and the companion fainter than in epochs E1–E5 and is another example of substantial departure from what might be expected in the case that AB Aur b is a disk feature seen in scattered light.

The Pearson sample correlation coefficient between the host and companion for E1–E5 is  $r=0.49$  with a relatively large confidence interval of  $\sigma_r=0.59$  using bootstrap resampling to estimate an uncertainty and  $\sigma_r=0.32$  using jackknife resampling; both approaches give comparably broad ranges that are consistent with no correlation. However, the correlation coefficient should be treated with caution because the number of measurements (five) is much smaller than is generally recommended for a robust interpretation of this metric (Bujang & Baharum 2016). Moreover, the large uncertainties are consistent with both strong positive correlation ( $r=1$ ) and complete independence of each parameter ( $r=0$ ) within about  $1\sigma$ .

#### 4.4. H $\alpha$ Line Flux, Accretion Luminosity, and Mass Accretion Rate

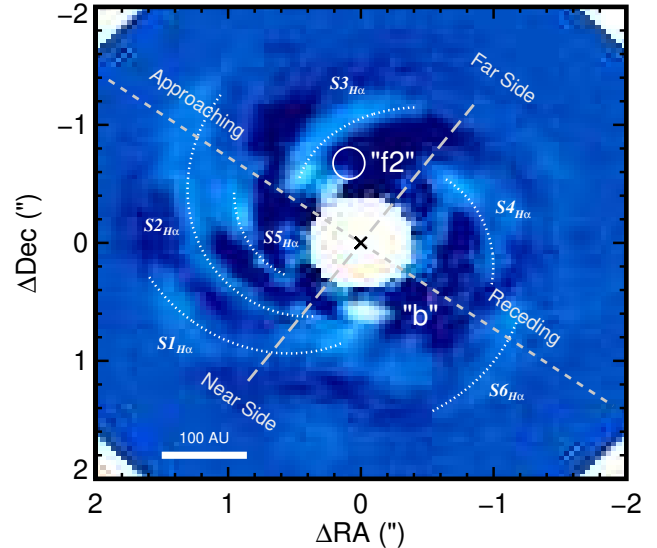


**Figure 7.** Coadded  $F656N$  image of AB Aur with HST. Observations represent the average of 6 epochs (E0–E5) of high-contrast imaging in H $\alpha$ , amounting to a total integration time of 2.5 hr from 25 orbits over two years (2022–2024). The short-dashed line is the line of nodes—the intersection of the sky and disk planes—and the long-dashed line is the projected rotation axis of the disk based on ALMA and NOEMA observations (Tang et al. 2017; Rivière-Marichalar et al. 2020). The disk is rotating counter-clockwise, with the north-east portion approaching and the south-east portion receding. AB Aur b (Currie et al. 2022; Zhou et al. 2022) is readily visible south of AB Aur (black  $\times$ ), but the point source  $f2$  north of AB Aur from Boccaletti et al. 2020 is not recovered. Known H $\alpha$  spiral features ( $S1_{H\alpha}$ – $S4_{H\alpha}$ ) and new scattered-light disk structures ( $S5_{H\alpha}$  and  $S6_{H\alpha}$ ) are labeled. No new H $\alpha$  point sources are identified.

Accretion luminosities and mass accretion rates can be derived from the observed H $\alpha$  emission of AB Aur and AB Aur b. For each epoch, flux densities in  $F656N$  from Table 2 are corrected for extinction assuming a reddening of  $A_V=0.51$  mag to AB Aur (McJunkin et al. 2014). The Fitzpatrick (1999) Galactic extinction curve and a ratio of total to selective extinction of  $R_V=3.1$  are adopted. For AB Aur, the contribution of the stellar continuum to the  $F656N$  photometry is removed by scaling a  $T_{\text{eff}}=9800$  K and  $\log g=4.0$  dex (Soubiran et al. 2016) PHOENIX/Gaia model atmosphere (Brott & Hauschildt 2005) to the  $V$ -band photometry of AB Aur, carrying out synthetic photometry with the HST  $F656N$  transmission curve (which yields a monochromatic flux density of  $2.07 \times 10^{-12}$  erg $^{-1}$  s $^{-1}$  cm $^{-2}$  Å $^{-1}$ ), and subtracting this from the extinction-corrected values. The resulting H $\alpha$  line flux and corresponding H $\alpha$  line luminosity ( $L_{H\alpha}$ ) adopting a Gaia DR3 distance of  $155.9 \pm 0.9$  pc is reported for each epoch in Table 3.

Note that this treatment of accretion luminosity assumes that chromospheric  $H\alpha$  emission is negligible in comparison at this early evolutionary phase of growth (e.g., Manara et al. 2017).

Accretion luminosity ( $L_{\text{acc}}$ ) can be inferred using empirical trends between  $L_{H\alpha}$  and  $L_{\text{acc}}$ . Using the  $L_{H\alpha}$ - $L_{\text{acc}}$  relation from Mendigutía et al. (2011), which is calibrated for Herbig AeBe stars, yields accretion luminosities between  $\log(L_{\text{acc}}/L_{\odot}) = 1.1$  and 1.2 for AB Aur, with a weighted mean of  $\log(L_{\text{acc}}/L_{\odot}) = 1.12 \pm 0.12$  across the six HST epochs. The mass accretion rate can then be found from  $L_{\text{acc}} = GM_*\dot{M}/R_*$ . Assuming a stellar mass of  $M_* = 2.4 \pm 0.2 M_{\odot}$  (DeWarf et al. 2003) and a radius of  $R_* = 2.96 \pm 0.08 R_{\odot}$  (Stassun et al. 2019) yields an average mass accretion rate of  $\log(\dot{M}/(M_{\odot} \text{ yr}^{-1})) = -6.28 \pm 0.12$  and a range of  $-6.3$  to  $-6.2$ . These values are similar to previous measurements for AB Aur: Garcia Lopez et al. (2006) found  $\log(L_{\text{acc}}/L_{\odot}) = 0.63$  and  $\log(\dot{M}/(M_{\odot} \text{ yr}^{-1})) = -6.85$ , Wichittanakom et al. (2020) found  $\log(L_{\text{acc}}/L_{\odot}) = 1.32$  and  $\log(\dot{M}/(M_{\odot} \text{ yr}^{-1})) = -6.13$ , and Salyk et al. (2013) found  $\log(L_{\text{acc}}/L_{\odot}) = 0.5$  and  $\log(\dot{M}/(M_{\odot} \text{ yr}^{-1})) = -6.90$ .

Under the assumption we are actually witnessing accretion from a young planet, a mass accretion rate can similarly be derived for AB Aur b. The extinction-corrected  $H\alpha$  line luminosity of AB Aur b is mapped to accretion luminosity and mass accretion rate using two empirical correlations: the  $L_{H\alpha}$ - $L_{\text{acc}}$  relation of low-mass stars and brown dwarfs from Alcalá et al. (2017)<sup>9</sup> and the observed  $\dot{M}$ - $M$  relation of stellar and substellar objects identified by Betti et al. (2023). A radius of  $2 R_{\text{Jup}}$  is assumed, which corresponds to the typical size of a giant planet or low-mass brown dwarf to within a factor of  $\sim 1.5$  at young ages ( $\lesssim 5$  Myr; e.g., Phillips et al. 2020). Using this value for the radius together with  $L_{\text{acc}}$  yields an expression for  $\dot{M}$  as a function of mass  $M$ :  $\dot{M} = RL_{\text{acc}}/(GM)$ . The intersection of this relation with the stellar/substellar  $\dot{M}$ - $M$  relation can be used to estimate a mass accretion rate and companion mass assuming AB Aur b follows this trend. Results are presented in Table 3; the average implied accretion luminosity is  $\log(L_{\text{acc}}/L_{\odot}) = -3.25$  and the average accretion rate is  $\log(\dot{M}/(M_{\odot} \text{ yr}^{-1})) = -11.0$ . The average value of  $\log(M\dot{M} / (M_{\odot}^2 \text{ yr}^{-1}))$  is  $-12.6$ . The corresponding average companion mass is  $34 M_{\text{Jup}}$ , which is

higher than estimates of  $9\text{--}12 M_{\text{Jup}}$  for AB Aur b from Currie et al. (2022). Note that because these are not direct measurements of the bolometric accretion luminosity, and because the host star likely contributes to the observed  $F656N$  flux from AB Aur b (see Section 4.5), these values should be treated with caution.

#### 4.5. Both Accretion Luminosity and Scattered Light?

Zhou et al. (2023) found that the UV through red-optical emission from AB Aur b shows the strong Balmer break and is therefore dominated by reflected light from its host star. This implies that our  $F656N$  photometry from AB Aur b may also include a significant contribution of underlying photospheric and  $H\alpha$  emission from AB Aur. In this scenario, some fraction of reflected light originates from the host, which is combined with strong variability produced by an accreting planet flickering in  $H\alpha$ .

We can estimate this contribution of the host star by comparing the  $F645N$  continuum photometry of AB Aur and AB Aur b from Zhou et al. (2023). The corresponding brightness ratio is 0.00032. If we apply this to the extinction-corrected  $H\alpha$  photometry of AB Aur so as to scale it down to the expected reflected-light  $H\alpha$  intensity, the resulting flux densities are broadly similar to the observed values for AB Aur b. In particular, the ratio between the observed flux density of AB Aur b and the scaled down brightness of AB Aur is  $0.76 \pm 0.10$ ,  $1.75 \pm 0.08$ ,  $0.60 \pm 0.08$ ,  $0.66 \pm 0.09$ ,  $2.5 \pm 0.16$ , and  $1.6 \pm 0.09$  for epochs E0 through E5, respectively. In this scenario, values above 1.0 would indicate that the  $F656N$  emission from AB Aur b is dominated by emission from the companion, while values near 1.0 imply that the emission is primarily reflected light from the host star. Values below 1.0 imply that the observed flux is less than the scaled host star contribution, probably a sign that the scaling factor based on the  $F645N$ -band observations is not constant over time. It could also indicate extinction is severe or variable. These ratios appear to fluctuate about 1, with the highest value of 2.5 corresponding to Epoch 4. This could be a result of real variations from AB Aur b, whereby stochastic accretion sometimes elevates the source brightness substantially above the reflected light contribution.

#### 4.6. Disk Features and Limits on $H\alpha$ Sources

These sensitive HST observations offer an opportunity to search for faint signals in  $H\alpha$  associated with AB Aur, including scattered light disk features and young accreting planets. Figure 7 shows the coadded image of all 6

<sup>9</sup> Note that Aoyama et al. (2021) propose an alternative theoretical  $L_{H\alpha}$ - $L_{\text{acc}}$  relation that may be more appropriate for embedded protoplanets experiencing accretion shocks. They predict a higher  $L_{\text{acc}}$  for a given  $L_{H\alpha}$ , which would imply a dramatically higher accretion luminosity and accretion rate for AB Aur b.

**Table 3.** Extinction-Corrected Photometry, H $\alpha$  Line Luminosity, and Mass Accretion Rate

Epoch ID	EC $f_\lambda$ <sup>a</sup> ( $10^{-15}$ erg s $^{-1}$ cm $^{-2}$ Å $^{-1}$ )	$F_{H\alpha}$ ( $10^{-10}$ erg s $^{-1}$ cm $^{-2}$ )	log $L_{H\alpha}$ ( $L_\odot$ )	log $L_{\text{acc}}$ <sup>b</sup> ( $L_\odot$ )	log $\dot{M}$ <sup>c</sup> ( $M_\odot$ yr $^{-1}$ )
AB Aur					
E0	10490 $\pm$ 170	1.48 $\pm$ 0.03	-0.95 $\pm$ 0.01	1.2 $\pm$ 0.3	-6.2 $\pm$ 0.3
E1	8516 $\pm$ 5	1.134 $\pm$ 0.0009	-1.064 $\pm$ 0.007	1.1 $\pm$ 0.3	-6.3 $\pm$ 0.3
E2	8655 $\pm$ 14	1.159 $\pm$ 0.003	-1.055 $\pm$ 0.007	1.1 $\pm$ 0.3	-6.3 $\pm$ 0.3
E3	7884 $\pm$ 17	1.023 $\pm$ 0.003	-1.109 $\pm$ 0.007	1.1 $\pm$ 0.3	-6.3 $\pm$ 0.3
E4	8895 $\pm$ 9	1.201 $\pm$ 0.002	-1.039 $\pm$ 0.007	1.1 $\pm$ 0.3	-6.3 $\pm$ 0.3
E5	7727 $\pm$ 13	0.996 $\pm$ 0.002	-1.121 $\pm$ 0.007	1.1 $\pm$ 0.3	-6.3 $\pm$ 0.3
AB Aur b <sup>d</sup>					
E0	2.3 $\pm$ 0.3	4.0 $\pm$ 0.5 $\times 10^{-4}$	-4.51 $\pm$ 0.05	-3.35 $\pm$ 0.06	-11.1 $\pm$ 0.7
E1	4.3 $\pm$ 0.2	7.5 $\pm$ 0.4 $\times 10^{-4}$	-4.24 $\pm$ 0.02	-3.05 $\pm$ 0.02	-10.9 $\pm$ 0.7
E2	1.5 $\pm$ 0.2	2.7 $\pm$ 0.4 $\times 10^{-4}$	-4.68 $\pm$ 0.06	-3.55 $\pm$ 0.06	-11.2 $\pm$ 0.7
E3	1.5 $\pm$ 0.2	2.7 $\pm$ 0.3 $\times 10^{-4}$	-4.69 $\pm$ 0.04	-3.56 $\pm$ 0.05	-11.3 $\pm$ 0.7
E4	6.5 $\pm$ 0.4	11.4 $\pm$ 0.8 $\times 10^{-4}$	-4.06 $\pm$ 0.03	-2.85 $\pm$ 0.03	-10.8 $\pm$ 0.7
E5	3.5 $\pm$ 0.2	6.2 $\pm$ 0.4 $\times 10^{-4}$	-4.33 $\pm$ 0.03	-3.15 $\pm$ 0.03	-11.0 $\pm$ 0.7

<sup>a</sup>EC refers to extinction-corrected values assuming  $A_V=0.51$  mag (McJunkin et al. 2014).

<sup>b</sup>For AB Aur, the  $L_{H\alpha}$ - $L_{\text{acc}}$  relation from Mendigutía et al. (2011) is used to derive accretion luminosity. For AB Aur b,  $L_{\text{acc}}$  is derived from  $L_{H\alpha}$  following Alcalá et al. (2017).

<sup>c</sup>For AB Aur, mass accretion rate is derived assuming a stellar mass of  $2.4 \pm 0.2 M_\odot$  from DeWarf et al. (2003) and a radius of  $2.96 \pm 0.08 R_\odot$  from Stassun et al. (2019). For AB Aur b, mass accretion rate is inferred from the stellar and substellar  $\dot{M}$ - $M_*$  trend from Betti et al. (2023).

<sup>d</sup>We emphasize that there is considerable uncertainty associated with our inferred values of  $L_{\text{acc}}$  and  $\dot{M}$  for AB Aur b. See Section 4.4 for details.

epochs of observations taken in *F656N* (E0–E5), which represents 2.5 hours of total integration time across 25 orbits. As far as we are aware, this is the deepest high-contrast imaging of AB Aur in H $\alpha$  to date. Although these combined individual reductions are not optimized to bring out extended emission and minimize self subtraction (e.g., Mazoyer et al. 2020; Flasseur et al. 2021; Pairet et al. 2021; Juillard et al. 2023), many known structures associated with the disk are evident. For consistency with previous work in this bandpass, we adopt the same naming convention for the spiral arm features from Zhou et al. (2022) with subscript  $H\alpha$  appended to avoid ambiguity with other spiral arm features on larger scales (e.g., Hashimoto et al. 2011; Speedie et al. 2024).

The most prominent structures are  $S1_{H\alpha}$ ,  $S2_{H\alpha}$ ,  $S3_{H\alpha}$ , and  $S4_{H\alpha}$ , each of which span several hundred AU in scale and radiate outward in the same direction—clockwise at increasing separations. In addition, we also identify the persistent structures  $S5_{H\alpha}$  and  $S6_{H\alpha}$  which are visible in this image but were not significant in previous shallower H $\alpha$  observations. The brightest of these features are also visible in HST UV-through-optical imaging of the system from Zhou et al. (2023), and high-resolution VLT/SPHERE near-infrared imaging (e.g., Boccaletti et al. 2020; Currie et al. 2022). The

orientation of the spiral arms are consistent with the disk kinematics from Tang et al. (2017); the disk is rotating in the counterclockwise direction and the spiral arms are trailing the bulk motion of the gas disk.

No point-like H $\alpha$  sources are evident within or immediately outside the scattered light disk ( $< 2''$ ). There have been several planet candidates noted within the AB Aur disk, but many of these are within the effective inner working angle of  $\approx 0''.4$  in our observations where contrasts are poor and PSF subtraction is unreliable. In particular, Boccaletti et al. (2020) identified two compact sources at sub-arcsecond separations in polarized and unpolarized  $H$ -band observations with VLT/SPHERE. Source *f1* is located  $0''.16$  south of AB Aur and is associated with extended emission and a twist in the inner spiral structure at tens of AU, which may be related to interactions between a young planet and the inner disk. *f1* is too close to AB Aur to reliably search for excess H $\alpha$  emission in these datasets.

The point source *f2* is located  $0''.681$  north of AB Aur near the inner edge of the transition disk. We do not recover *f2* in H $\alpha$ , although the neighboring spiral feature just north of *f2* that is present in the Boccaletti et al. (2020) observations is also recovered in our HST observations ( $S3_{H\alpha}$ ). Similarly, hints of the curved, trailing

tip of their “S1” inner spiral are visible in  $H\alpha$  immediately south-east of the expected position of  $f2$ . Both  $f1$  and  $f2$  are detected in polarized-intensity observations from Boccaletti et al. (2020); as a result, they conclude that these sources most likely correspond to scattering from dust in the disk. The morphology of  $f1$  and its relationship to the inner spiral arms are most closely connected to expectations of an embedded young planet, whereas  $f2$  may instead be structure within the disk. If  $f2$  is actually a protoplanet, the lack of  $H\alpha$  emission indicates that it is embedded with a high extinction or it is not accreting.

No  $H\alpha$  sources are evident at wider separations. The  $3\sigma$  upper limit in an annulus from  $1''.75$ – $2''.56$  (270–400 AU) is  $0.046 \text{ e}^- \text{ s}^{-1}$ , or  $f_\nu = 0.0033 \text{ mJy}$  ( $f_\lambda = 2.3 \times 10^{-18} \text{ erg s}^{-1} \text{ cm}^{-2} \text{ \AA}^{-1}$ ). Assuming a reddening of  $A_V=0.51 \text{ mag}$  to AB Aur (McJunkin et al. 2014), the upper limit corrected for extinction is  $f_\lambda = 3.2 \times 10^{-18} \text{ erg s}^{-1} \text{ cm}^{-2} \text{ \AA}^{-1}$ . Using the  $F656N$  filter width of  $\Delta\lambda = 17.6 \text{ \AA}$ , this corresponds to an upper limit on the  $H\alpha$  line flux of  $5.7 \times 10^{-17} \text{ erg s}^{-1} \text{ cm}^{-2}$ . At the distance to AB Aur (155.9 pc), the limit on the line luminosity is  $1.7 \times 10^{26} \text{ erg s}^{-1}$ , or  $4.3 \times 10^{-8} L_\odot$ .

## 5. DISCUSSION

The results of this accretion light echo experiment offer two main insights about AB Aur b: the scenario of stable scattering of  $H\alpha$  emission from the host star is not supported by our HST observations (Figure 6), and large-amplitude variability is occurring over timescales of weeks to years. This implies that the variability originates very close to either the star or the companion where dynamical timescales are short. Below we discuss these interpretations in more detail. In Section 5.1 we compare the variability of AB Aur b with what is known about the timescales and amplitudes of accretion in the planetary domain. Alternative interpretations unrelated to an accreting planet are discussed in Section 5.2.

### 5.1. How Common is AB Aur b-like Variability?

The factor of four variation in brightness from AB Aur b implies a proportional change in the  $H\alpha$  line flux and—if it is indeed a protoplanet—accretion luminosity, assuming the same fraction of  $L_{\text{acc}}$  emerges in  $H\alpha$  across all epochs of this program. How typical is this scale of variability compared to other accreting planets, and can this lend insight into the nature of AB Aur b? Here we contrast the high level of  $H\alpha$  variability of AB Aur b with other young planets and widely separated planetary-mass companions. Although the immediate surroundings and evolutionary phase of AB Aur b differ from other well-studied systems, this comparison nevertheless provides context for whether the  $H\alpha$  variability

behavior of AB Aur b is largely consistent or discrepant with what is known about accretion in the planetary domain.

#### 5.1.1. Comparison with PDS 70 b and c

The most prominent uncontested examples of accreting protoplanets are the young giant planets PDS 70 b and c. The most measurements in  $H\alpha$  have been made for PDS 70 b, the inner of the two imaged planets. PDS 70 b was first imaged in  $H\alpha$  by Wagner et al. (2018) using Magellan/MagAO, and since then has been followed up by Haffert et al. (2019) with VLT/MultiUnit Spectroscopic Explorer—observations that were subsequently reanalyzed by Hashimoto et al. 2020—and HST/WFC3 (Zhou et al. 2021). More recently, Close et al. (2025) report multi-year observations of the PDS 70 planets in  $H\alpha$  with Magellan/MagAO-X, and Zhou et al. (2025, in press) present new HST observations of the system; these are discussed in detail below.

Zhou et al. (2021) carried out an analysis of  $H\alpha$  variability of PDS 70 b up to that point. There are some signs of modest brightness changes at  $3.5\sigma$ , but they rule out significant variability at the  $>30\%$  level. They also note that the possible brightness changes could instead be caused by unaccounted-for systematic biases associated with the variety of instruments, observing strategies, and post-processing techniques used in these studies.

This picture for both PDS 70 b and c has recently come into focus with results from Close et al. (2025) and Zhou et al. (2025, in press). Close et al. (2025) recovered PDS 70 b and c from MagAO-X observations in  $H\alpha$  from 2022 to 2024. PDS 70 b decreased by a factor of 4.6 and PDS 70 c increased by a factor of 2.3 during this timeframe. By 2024, PDS 70 c appeared brighter than b, indicating long-term trends related to evolving mass accretion. Zhou et al. find similar results with new HST imaging in  $H\alpha$ ; both planets are recovered in observations from 2024 and a clear brightening of PDS 70 c is detected when compared with observations from 2020. Altogether this points to variations on year-long timescales with amplitudes that are broadly similar to what we find for AB Aur b, although the timescales of brightening and fading appear to be longer for the PDS 70 planets than for AB Aur.

It is possible that these differences might be attributed to distinct evolutionary stages of protoplanetary growth between PDS 70 b, PDS 70 c, and AB Aur b. The inferred accretion rate of  $\dot{M} \approx 10^{-8} M_{\text{Jup}} \text{ yr}^{-1}$  (Wagner et al. 2018; Haffert et al. 2019; Hashimoto et al. 2020; Zhou et al. 2021; Close et al. (2025); Zhou et al. 2025, in press) implies that PDS 70 b and c are near the end



of their primary phase of growth, and their accretion luminosity is about 300 times lower than what was inferred for AB Aur b in Section 4.4. However, if AB Aur b is indeed an accreting protoplanet, the extended nature of the source suggests that it may be embedded within AB Aur’s protoplanetary disk, perhaps with an extended envelope and large circumplanetary disk. If there is a correlation between the rate of mass accretion and level of variability, then the earlier evolutionary stage of AB Aur b compared to PDS 70 b and c could also explain potential differences between the observed variability properties of these two case studies. A clearer understanding of the variability properties of protoplanets will be needed to map the behavior of accretion over time.

### 5.1.2. Comparison with Accreting Planetary-Mass Companions

Active accretion, hydrogen line emission, and circumplanetary disks are common among long-period giant planets and low-mass brown dwarf companions orbiting young stars. Bowler et al. (2017) found that at least half of widely separated ( $\gtrsim 100$  AU) substellar companions with masses below  $\approx 20 M_{\text{Jup}}$  and ages  $\lesssim 15$  Myr show Pa $\beta$  emission. Owing to the wavelength dependence of dust absorption, this near-infrared line is less sensitive to extinction and potential confusion with chromospheric activity compared to H $\alpha$  and implies ongoing mass accretion. Martinez & Kraus (2022) found a comparable lower limit on the occurrence rate of circumplanetary disks based on thermal excess emission.

How useful is this population as a comparison sample for AB Aur b? Based on their orbital eccentricities, stellar obliquities, and atmospheric compositions, there is growing evidence that the dominant origin of wide planetary companions is more aligned with gravitational fragmentation of molecular cloud cores or protoplanetary disks compared to core- or pebble-accretion channels typically associated with giant planets at closer separations (e.g., Wu et al. 2017; Pearce et al. 2019; Bowler et al. 2020; Bryan et al. 2021; Palma-Bifani et al. 2022; Bowler et al. 2023; Balmer et al. 2024; Xuan et al. 2024). Nevertheless, despite their older ages compared to AB Aur b, the high prevalence of subdisks among these objects and relative ease of moderate-resolution spectroscopy has opened the door to regular spectroscopic monitoring spanning a variety of timescales. In this sense, if AB Aur b is a young planet, it could represent an example of a younger analog of these objects.

Recently, Demars et al. (2023) carried out a detailed analysis of the Pa $\beta$  emission line variability for two widely-separated companions near the deuterium-burning limit, GQ Lup B and GSC 0614-210 b. They

found that variability is typically modest on short timescales of hours to weeks but dramatically increases to 100–1000% on timescales of years to decades. Other studies have come to similar conclusions in the substellar regime. Stelzer et al. (2007) identified order-of-magnitude variability on timescales of months to years from the brown dwarf host 2MASS J12073346–3932539 A. Wu et al. (2023) found that H $\alpha$  variability of the  $\approx 19 M_{\text{Jup}}$  companion FU Tau B is relatively low (10–20%) on short timescales of hours to days. Wolff et al. (2017) showed that the Pa $\beta$  emission line of DH Tau B varies by a factor of a few on timescales of weeks to months. In the thorough compendium of accreting objects spanning stars to planets, Betti et al. (2023) found that the spread of  $\approx 100$ –300% in accretion variability down to the deuterium-burning limit is not particularly unusual compared to trends among brown dwarfs and stars.

There is clearly a large dynamic range of variability amplitudes among accreting giant planets and wide planetary-mass objects. These broadly correlate with sampling timescales, with higher variability observed over longer time baselines. This variability amplitude and timescale is consistent with what we find for AB Aur b, given our limited sampling. We conclude that if the observed H $\alpha$  of AB Aur b originates from accretion onto a protoplanet, the observed variability is within the range of accreting wide-orbit planetary mass companions. We also note that this variability could impact population statistics from direct imaging surveys searching for accreting young planets using emission lines (Plunkett et al. 2024), as young planets may be missed during quiescent phases of accretion. Multiple epochs over long timescales could help overcome this possible bias in protoplanet demographics.

## 5.2. Alternative Interpretations

### 5.2.1. Variable Extinction?

Changes in the H $\alpha$  line luminosity, accretion luminosity, and mass accretion rate discussed in Section 4.4 inherently assume the observed variations relate to stochastic accretion. However, the H $\alpha$  variability from AB Aur b could alternatively be caused by evolving line-of-sight extinction from accretion flows, circumplanetary material, or circumstellar material, altering what may actually be a more constant mass accretion rate onto a young planet (e.g., Marleau et al. 2022).

The circumplanetary environment surrounding a protoplanet is expected to be complex, but there are few observational constraints to help anchor the picture of giant planet growth at the earliest embedded stages. The immediate region near a growing planet is likely to in-

clude a circumplanetary disk out to an appreciable fraction of the Hill radius (e.g., Ward & Canup 2010; Fung et al. 2019; Taylor & Adams 2024; Zhu 2015). Prior to a gap-opening phase when circumstellar disk surface densities diminish, the circumplanetary disk may take the form of a decretion disk with gas circulating via meridional flows and accretion proceeding along the polar regions (Tanigawa et al. 2012; Batygin 2018; Szulágyi et al. 2022). Magnetically driven outflows from a young planet might accompany this process (Quillen & Trilling 1998; Fendt 2003; Law et al. 2023; Yoshida et al. 2024). All of this can give rise to variable extinction to the growing planet.

What are the implied extinction values given the observed variability of AB Aur b? Taking the brightest epoch (E4) of AB Aur b as a reference point, we can deredden the other measurements of AB Aur b at other epochs until we reach this value. The resulting extinctions are  $\Delta A_V = 1.5$  mag, 0.6 mag, 2.1 mag, 2.1 mag, and 0.9 mag for epochs E0, E1, E2, E3, and E5, respectively, using the reddening law from Fitzpatrick (1999). Given the timing of the observations, with E1–E3 taken within a two-month period in 2023 and E4 and E5 taken within a two-week period in 2024, this would indicate that changes in extinction at the scale of 1–2 magnitudes is occurring on timescales of weeks to months.

It is unclear whether these constraints on the timescale and amplitude of variations alone can be used as a meaningful test of this variable extinction hypothesis because of the potential complexity of the circumplanetary region. Each physical process will operate on its own characteristic timescale—Keplerian motion of a disk about the planet, high-velocity outflows expelling gas and entraining dust, accretion and meridional flows, and the planetary rotation rate. Some other relevant timescales are discussed in Chiang & Goldreich (1997). Of course, it is also possible that both extinction and changes in accretion luminosity could both be taking place simultaneously, which would be challenging to disassociate.

### 5.2.2. Inner Disk Shadowing?

The dissimilar variability between AB Aur A and b has thus far been discussed in the context of AB Aur b as an accreting planet. However, there are other plausible, and perhaps even likely, explanations for the inconsistent variability between AB Aur and AB Aur b that are unrelated to emission from a young planet. These alternative interpretations should be considered alongside the planet hypothesis.

One possibility is that AB Aur b is a compact disk feature seen in scattered light and that brightness variations are caused not by the source itself, but from struc-

tural changes in the inner disk located along the sight line from AB Aur b to its host star. This type of inner disk shadowing is becoming increasingly recognized as a common phenomenon among protoplanetary disks with dynamic inner regions. Examples of shadowing structures include inner disk misalignments (e.g., Benisty et al. 2018; Pinilla et al. 2018; Zhu 2018; Bohn et al. 2022; Debes et al. 2023; Villenave et al. 2024), warps (Nealon et al. 2019; Kluska et al. 2020), “puffed up” inner disk walls with variable scale heights (Sitko et al. 2008; Wisniewski et al. 2008; Muzerolle et al. 2009), dust transport caused by magnetic activity close to the star (Turner et al. 2010), and dust entrained in outflows from the inner disk (Liffman et al. 2020). Some of this inner disk evolution is expected to be connected to orbiting planets, which can perturb the nearby disk structure not just in the disk’s midplane but also in its vertical structure. Indeed, several planet candidates have been identified in the inner regions of the AB Aur disk (Boccaletti et al. 2020) which could be related to the observed variability of AB Aur b if they can impact the disk structure at sub-AU scales.

What adds more credence to this picture is that the AB Aur disk has itself been shown to exhibit brightness variations. Shenavrin et al. (2019) found in unresolved imaging observations that AB Aur is variable by up to 0.7 mag from 1–5  $\mu\text{m}$  where inner disk emission dominates over the stellar photosphere (see also Shenavrin et al. 2012). At longer wavelengths, Prusti & Mitsukevich (1994) identified brightness changes of 0.27 mag at 12  $\mu\text{m}$  and 0.17 mag at 25  $\mu\text{m}$  with IRAS over a 6-month period. Chen & Jura (2003) measured comparable variability at the 20–50% level at 11.7  $\mu\text{m}$  and 18.7  $\mu\text{m}$  from observations at Keck Observatory. This temporal variability is suggestive of changing disk illumination, although the origin and specific nature of the variability is unclear given the limited long-wavelength monitoring of AB Aur.

An outer limit of the location of shadowing can be estimated from the minimum timescale over which variability is observed. For this dataset, this occurs between Epochs 4 and 5, which are separated by about 12 days. Assuming a stellar mass of  $2.4 M_\odot$ , this corresponds to an orbital distance of 0.14 AU. Physical variations of the inner disk are expected at smaller spatial scales, so in this scenario shadowing is likely to originate closer in. Moreover, this estimate is limited by sampling cadence; shorter timescale variability would imply vertical structure at even shorter orbital periods.

The inner regions of AB Aur’s disk have been probed at high spatial resolution with optical and near-infrared interferometry (e.g., Millan-Gabet et al. 2001; Eisner

et al. 2004; Millan-Gabet et al. 2006; Tannirkulam et al. 2008a). In a comprehensive modeling effort by Tannirkulam et al. (2008b), they found an inner dust disk with an inner radius of 0.24 AU, which is similar to spatial scales of resolved structures identified with interferometry. The dynamical (Keplerian) timescale at this separation is of order a month, and any inhomogeneities of the inner disk could result in changes to shadowing on much shorter times of only a fraction of the orbital period. This is broadly consistent with our observations of AB Aur b, suggesting that inner shadowing of inner disk structure could plausibly explain the observed variability.

Finally, there are also signs that the AB Aur disk exhibits a global warp based on inclination measurements from small separations out to large spatial scales corresponding to the outer disk (Hashimoto et al. 2011; Tang 2012; Speedie et al. 2024). The origin of the warp is unclear, but may be related to a close-in inclined planet similar to behavior in the  $\beta$  Pic disk (e.g., Mouillet et al. 1997; Apai et al. 2015). Disk warps can also result from the dynamical influence on an outer companion. AB Aur is a wide binary with the nearby disk-bearing star SU Aur (e.g. Herbig 1960; Eggen 1975; DeWarf et al. 2003), but the projected separation of 26,800 AU is likely too large to significantly impact AB Aur’s disk<sup>10</sup>. Regardless, precession of a warped inner disk can also contribute to variability of the outer disk and could be connected to the observed H $\alpha$  brightness changes.

### 5.2.3. A Dynamic Disk Feature?

Another way in which a compact disk feature could result in variability is if the structure itself is evolving, and in the process changing the effective scattered light surface area along our line of sight. An overdensity in the disk can experience a change in morphology through a range of processes including shearing as a result of orbital motion or heating from exposure to stellar irradiation. There are many examples of evolving small-scale disk features, which are often located at small spa-

tial scales in regions vulnerable to heating from the star (Huélamo et al. 2011; Olofsson et al. 2011; Kraus & Ireland 2012; Cheetham et al. 2015; Sallum et al. 2015b; Sallum et al. 2015a; Follette et al. 2017; Gratton et al. 2019). Recently, Sallum et al. (2023) found evidence of small-scale structures in the LkCa 15 disk at  $\sim 20$  AU that are undergoing both brightness and morphological changes on timescales of years. This may be what we are witnessing with AB Aur.

### 5.3. Testing These Scenarios

Here we comment on a few observational tests that might be used to distinguish these scenarios. Differential emission line profiles and velocities between AB Aur A and b would be a telltale signature of a planet, as the freefall velocity of accreting gas falling onto a massive star should be substantially broader than the velocity wings for a planet. This approach was used by Haffert et al. (2019) to argue that PDS 70 b and c are both accreting planets based on their H $\alpha$  emission line widths, shapes, and velocity offsets. Like PDS 70, the H $\alpha$  emission line from AB Aur shows an inverse P Cygni profile, and in principle could be used to discriminate these scenarios. However, this is complicated by the scattered-light contribution of AB Aur, which may be substantial (Section 4.5), and the wide orbital distance implies a velocity offset of only a few km s<sup>-1</sup>.

Another approach to distinguish these scenarios is to simultaneously monitor AB Aur b variability in the H $\alpha$  line and a neighboring continuum region. Changing shadows or a dynamic disk feature should impact both continuum and line emission in the same way, whereas a constant continuum but changing H $\alpha$  line strength would point to an accreting planet. Furthermore, accretion luminosity and extinction can potentially be separated through simultaneous monitoring of multiple accretion tracers in the near-infrared where extinction is lower, for instance with Paschen or Brackett series recombination emission lines (e.g., Biddle et al. 2024; Marleau et al. 2024). Variable extinction would alter line ratios as a function of wavelength, while variable mass accretion would impact overall line intensities.

Tracking H $\alpha$  brightness variations at other positions within the AB Aur scattered light disk can also be used to determine whether the observed variability from AB Aur b is typical or unique to this source. Distinct changes from AB Aur b would provide strong evidence that it is a planet if the rest of the disk varies in sync. However, a careful accounting of the light echo effect at other locations is required, as an impulse of emission from the host star would reverberate at different times across the disk. It would also require careful for-

<sup>10</sup> This physical connection between AB Aur and SU Aur is strengthened with Gaia DR3 astrometry (Gaia Collaboration et al. 2022). AB Aur has a parallax of  $6.413 \pm 0.037$  mas and proper motions of  $\mu_\alpha \cos \delta = 4.02 \pm 0.04$  mas yr<sup>-1</sup> and  $\mu_\delta = -24.03 \pm 0.04$  mas yr<sup>-1</sup>. The parallax of SU Aur is 6.370  $\pm$  0.030 mas and proper motions of  $\mu_\alpha \cos \delta = 4.19 \pm 0.03$  mas yr<sup>-1</sup> and  $\mu_\delta = -24.30 \pm 0.02$  mas yr<sup>-1</sup>. Both stars have slightly elevated Gaia Renormalized Unit Weight Error (RUWE) values of 1.37 for AB Aur and 1.51 for SU Aur, which may be suggestive of a close-in companion (Stassun & Torres 2021), although Fitton et al. (2022) propose a higher RUWE threshold of 2.5 for young disk-bearing stars as a result of excess astrometric variability in these systems.

ward modeling of the disk to avoid the impact of self-subtraction—something that may be possible with this HST dataset but which is beyond the immediate goals of this study.

Finally, continued variability monitoring of AB Aur b over a wide range of timescales should offer further clues about the origin of the brightness changes. Short-cadence observations over days and weeks would sample rapid changes caused by mass accretion, inner disk features, and gas dynamics in the circumplanetary region. Over months and years, longer-term trends from slower processes connected to orbital motion of the planet or precession of a warped disk should be evident.

#### 5.4. Applications of Accretion Light Echoes

In this study, we use  $H\alpha$  images of the host star AB Aur to monitor its accretion luminosity prior to acquiring the deeper observations of the companion. Here the source geometry and light travel time to AB Aur b is known, but in other instances the orbital geometry of a planet candidate may be unknown or poorly constrained. In these scenarios, we recommend a long baseline of continuous  $H\alpha$  monitoring of the host star leading up to and during the high-contrast imaging observations. This could be carried out even with low-resolution optical spectroscopy, ideally commencing  $\sim 1.4 \times (r/(10 \text{ AU}))$  hours before the deep imaging, where  $r$  is the separation to the source in AU. This scaling corresponds to the maximum light travel time to a given orbital distance. For probing wide separations of order 100 AU, this may not be practical to carry out for ground-based telescopes at the same site or with the same facility because of the long light travel time. In this case longitudinal site coverage may help—for instance, spectroscopic monitoring from Chile prior to deep  $H\alpha$  imaging from Hawai'i. Long delay times may be more practical for space-based facilities such as HST.

In principle, an  $H\alpha$  light curve of a variable host star and companion could be used not just to validate or refute a candidate planet, but also to measure the stellocentric distances to features within a disk. With high enough cadence and a long time baseline of the companion, the time delay measured from a cross correlation of light curves at different positions in the disk would map disk structures in three dimensions—in essence, reverberation mapping of resolved disks. Much of this will be facilitated with the next generation of 25–40-meter telescopes with sensitivity to smaller spatial scales, fainter disk structures, and lower-mass protoplanets.

## 6. SUMMARY

Distinguishing compact disk features from accreting planets is a significant observational challenge. We have

presented a framework for using accretion light echoes to probe the nature of candidate accreting protoplanets around young stars. Well-timed  $H\alpha$  observations of the host star that take into account the light travel time to the companion offer a new approach to disentangle scattered light from planetary accretion luminosity through correlated brightness variations.

We applied this method to the candidate planet AB Aur b with five epochs of high-contrast  $H\alpha$  ( $F656N$ ) imaging using HST/WFC3. Each epoch sampled the host star's brightness prior to deep imaging of the candidate companion, with the delay time corresponding to the observed light travel time delay to AB Aur b. Below is a summary of our results.

- AB Aur b is recovered in all five epochs taken in 2023–2024. The source is spatially resolved with an average aspect ratio of  $\sigma_x/\sigma_y = 1.5$ . The elongation in the azimuthal direction, consistent with previous results with ground- and space-based imaging. The corresponding deprojected size of the AB Aur b structure is  $91 \text{ mas} \times 57 \text{ mas}$ , or  $14 \text{ AU} \times 9 \text{ AU}$ . We also reprocessed previous HST observations of AB Aur in  $H\alpha$  from Zhou et al. (2022) in a consistent fashion to compare with results from this program. This earlier dataset did not sample the host star with a time delay, but extends  $H\alpha$  photometric monitoring of AB Aur b with HST to two years.
- AB Aur b is highly variable at the 330% level while the host star exhibits more modest brightness changes of 15% during this monitoring campaign. Variations at the 100–200% level from AB Aur b are observed on timescales of weeks to months. This level of variability is not unusual for known accreting planetary-mass companions and free-floating giant planets on comparably long timescales.
- The variability between AB Aur A and b do not show strong covariance. This disagrees with expectations if AB Aur b is purely unobstructed, passive scattered emission. These results either bolsters evidence that AB Aur b is an accreting planet, or we are witnessing variations associated with a dynamic disk environment.
- Assuming the emission is entirely accretion luminosity from a protoplanet, we find an average  $H\alpha$  line luminosity of  $\log(L_{H\alpha}/L_{\odot}) = -4.4$ . Using the  $L_{H\alpha}-L_{\text{acc}}$  relation from Alcalá et al. (2017) yields an average accretion luminosity of  $\log(L_{\text{acc}}/L_{\odot}) = -3.25$ . We caution that this depends on many



unknown factors, most notably potential extinction associated with the immediate environment surrounding AB Aur b. Nevertheless, this is over two orders of magnitude higher than PDS 70 b (Zhou et al. 2021). This could reflect an earlier evolutionary state of AB Aur b with comparably higher mass accretion. However, Zhou et al. (2023) showed that emission from AB Aur b is certainly related to a spatially extended disk feature that is scattering emission from the host star. When taking this into account, some epochs appear to be dominated by reflected light from AB Aur A, while at other epochs AB Aur b outshines the host star’s contribution by up to a factor of 2.5 at maximum brightness. It is also possible that variable line-of-sight extinction to AB Aur b could contribute to its observed variability.

- If the AB Aur b feature is associated with a protoplanet then these results represent the highest level of H $\alpha$  variability of any imaged planet or wide planetary-mass companion to date. To avoid missing variable signals, it would be prudent for direct imaging surveys using accretion signatures like H $\alpha$  to carry out multi-epoch observations rather than a single epoch strategy, which might happen to sample a planet during a low state of mass accretion.
- Our coadded image of AB Aur amounts to 25 orbits, or about 2.5 hours of total integration time. To our knowledge, this is the deepest H $\alpha$  imaging of this system to date. AB Aur b is the most prominent source. We recover the brightest spiral features and detect new scattered-light substructures in the disk. No other point sources are detected at wider separations down to  $3\sigma$  upper limits of  $f_\lambda = 3.2 \times 10^{-18} \text{ erg s}^{-1} \text{ cm}^{-2} \text{ \AA}^{-1}$ .
- There are several alternative interpretations for AB Aur b that should be considered alongside the accreting planet hypothesis. It is possible that AB Aur b is simply the brightest scattered-light clump in a highly structured disk. There are many ways to induce brightness changes in this scenario. This includes shadowing caused by a misaligned inner disk, a puffed up inner disk wall, a disk warp, or inner disk outflows. Evolution of a compact dust structure can also result in brightness changes as the projected scattering surface area changes. Distinguishing the effects of extinction, changing illumination, inner disk scale height, and dynamic dust structures can be ad-

dressed with multiwavelength variability monitoring over a range of timescales.

- More broadly, accretion light echoes may be a useful tool to distinguish scattered light disk features from accreting protoplanets. Uniquely interpreting the H $\alpha$  variability can be challenging in complex disk environments like AB Aur, but this approach could complement other strategies to distinguish scattered-light and planetary hypotheses such as sensitive polarized intensity imaging and differential emission line profiles. To facilitate accretion light echo variability measurements, we recommend continuous spectroscopic monitoring of the host star to track accretion tracers prior to and throughout deep H $\alpha$  imaging observations.

We are grateful to the referee for their helpful feedback, Christopher McKee and Wenbin Lu for helpful conversations about light echoes, and Tricia Royle at STScI for support scheduling the HST observations with the appropriate time delay for this program. B.P.B. acknowledges support from the National Science Foundation grant AST-1909209, NASA Exoplanet Research Program grant 20-XRP20.2-0119, and the Alfred P. Sloan Foundation. This material is based upon work supported by the National Science Foundation Graduate Research Fellowship under Grant No. 2139433. This research is based on observations made with the NASA/ESA Hubble Space Telescope obtained from the Space Telescope Science Institute, which is operated by the Association of Universities for Research in Astronomy, Inc., under NASA contract NAS 5-26555. These observations are associated with programs GO 17168 and GO 16651. This research has made use of NASA’s Astrophysics Data System Bibliographic Services

*Facilities:* HST(WFC3), TESS

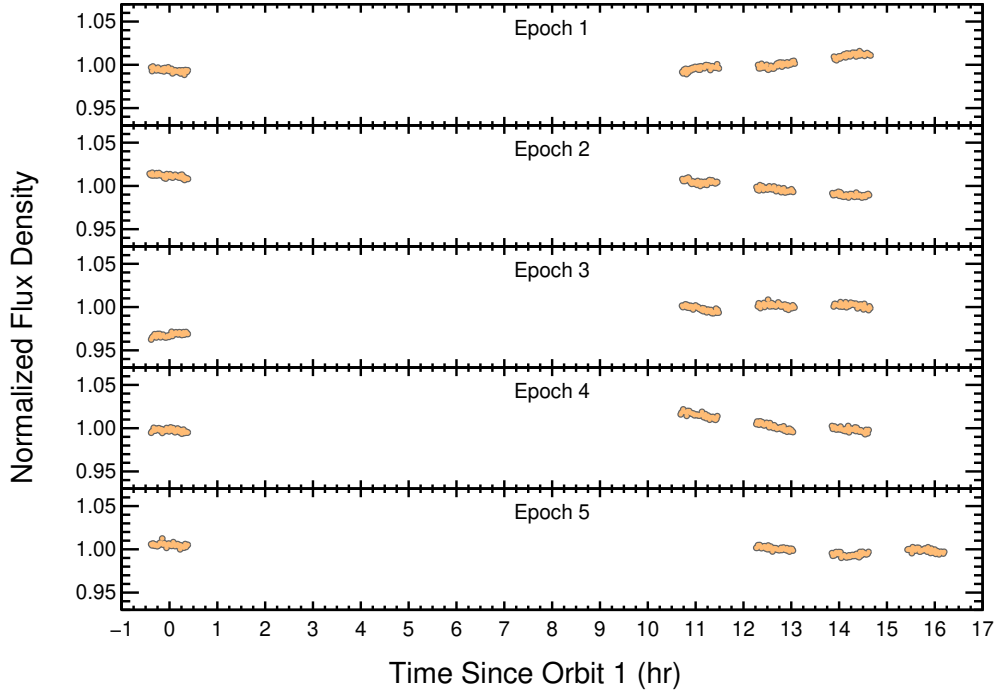


**Figure 8.** Light curves of AB Aur in  $F656N$  across the five epochs of this experiment. Light curve timescales are with respect to the midpoint of Orbit 1, and photometry has been normalized to the average flux in Orbit 1. Overall AB Aur is quite stable, with low-amplitude changes in  $H\alpha$  at the few-percent level evident across the 15–17 hour baseline of each epoch.

## APPENDIX

### A. LIGHT CURVES OF AB AUR

HST undergoes heating and settling cycles when its thermal environment changes. This can happen if HST’s orientation relative to the Sun is altered, for instance during the course of an orbit or when slewing between targets. The impact of thermal changes are small focal variations that can alter the PSF shape, encircled energy in the PSF core, and photometric measurements by a few percent (e.g., [Anderson & Bedin 2017](#)). The scale of these systematic effects is small compared to the observed brightness changes of AB Aur and AB Aur b. Here we examine whether there are signs of breathing patterns to determine what, if any, effect it might have on the photometry and uncertainties we have used in this work.

Section 3.3 describes our approach to extracting  $F656N$  photometry of AB Aur in Orbit 1 of each epoch and applying an aperture correction to account for flux loss at larger radii. We also measure photometry of AB Aur in each frame for Orbits 2–4 of each epoch in the same fashion. If breathing is impacting the light curves of AB Aur, we would expect this to have the greatest impact on Orbits 1 and 2, as these data are taken after slews from executing other programs.

The results are displayed in Figure 8. Intra-orbit  $H\alpha$  light curves are well behaved and show small, smoothly varying changes at the level of a few percent within a single orbit. Inter-orbit variability is comparable, with both positive and negative trends persisting for several orbits. The light curves undulate on few-hour timescales which is likely related to small changes in accretion rate. We also note that photometry from Orbit 1 is in good agreement with the light curves from Orbits 2–4. There are no signs of a persistent pattern in the light curve shapes from Orbits 1 and 2 that might be attributable to breathing and thermal stabilization.

## REFERENCES

- Alcalá, J. M., Manara, C. F., Natta, A., et al. 2017, *Astronomy & Astrophysics*, 600, A20, doi: [10.1051/0004-6361/201629929](https://doi.org/10.1051/0004-6361/201629929)
- Anderson, J., & Bedin, L. R. 2017, *MNRAS*, 470, 948, doi: [10.1093/mnras/stx1278](https://doi.org/10.1093/mnras/stx1278)
- Aoyama, Y., Ikoma, M., & Tanigawa, T. 2018, *The Astrophysical Journal*, 866, 0, doi: [10.3847/1538-4357/aadc11](https://doi.org/10.3847/1538-4357/aadc11)
- Aoyama, Y., Marleau, G.-D., Ikoma, M., & Mordasini, C. 2021, *The Astrophysical Journal Letters*, 917, 0, doi: [10.3847/2041-8213/ac19bd](https://doi.org/10.3847/2041-8213/ac19bd)
- Apai, D., Schneider, G., Grady, C. A., et al. 2015, *The Astrophysical Journal*, 800, 136, doi: [10.1088/0004-637x/800/2/136](https://doi.org/10.1088/0004-637x/800/2/136)
- Argyle, E. 1974, *Icarus*, 21, 199, doi: [10.1016/0019-1035\(74\)90138-9](https://doi.org/10.1016/0019-1035(74)90138-9)
- Bacon, R., Accardo, M., Adjali, L., et al. 2010, *Ground-based and Airborne Instrumentation for Astronomy III*, 773508, doi: [10.1117/12.856027](https://doi.org/10.1117/12.856027)
- Bahcall, J. N., Koslovsky, B.-Z., & Salpeter, E. E. 1972, *ApJ*, 171, 467
- Balmer, W. O., Pueyo, L., Lacour, S., et al. 2024, *The Astronomical Journal*, 167, 64, doi: [10.3847/1538-3881/ad1689](https://doi.org/10.3847/1538-3881/ad1689)
- Batygin, K. 2018, *The Astronomical Journal*, 155, 0, doi: [10.3847/1538-3881/aab54e](https://doi.org/10.3847/1538-3881/aab54e)
- Benisty, M., Juhász, A., Facchini, S., et al. 2018, *Astronomy & Astrophysics*, 619, A171, doi: [10.1051/0004-6361/201833913](https://doi.org/10.1051/0004-6361/201833913)
- Benisty, M., Bae, J., Facchini, S., et al. 2021, *The Astrophysical Journal Letters*, 916, 0, doi: [10.3847/2041-8213/ac0f83](https://doi.org/10.3847/2041-8213/ac0f83)
- Betti, S. K., Follette, K. B., Ward-Duong, K., et al. 2022, *The Astrophysical Journal Letters*, 935, L18, doi: [10.3847/2041-8213/ac85ef](https://doi.org/10.3847/2041-8213/ac85ef)
- . 2023, *The Astronomical Journal*, 166, 262, doi: [10.3847/1538-3881/ad06b8](https://doi.org/10.3847/1538-3881/ad06b8)
- Biddle, L. I., Bowler, B. P., Zhou, Y., Franson, K., & Zhang, Z. 2024, *The Astronomical Journal*, 167, 172, doi: [10.3847/1538-3881/ad2a52](https://doi.org/10.3847/1538-3881/ad2a52)
- Blakely, D., Francis, L., Johnstone, D., et al. 2022, *The Astrophysical Journal*, 931, 3, doi: [10.3847/1538-4357/ac6586](https://doi.org/10.3847/1538-4357/ac6586)
- Blandford, R. D., & McKee, C. F. 1982, *ApJ*, 255, 419
- Boccaletti, A., Folco, E. D., Pantin, E., et al. 2020, *Astronomy and Astrophysics*, 637, L5, doi: [10.1051/0004-6361/202038008](https://doi.org/10.1051/0004-6361/202038008)
- Bohn, A. J., Benisty, M., Perraut, K., et al. 2022, *Astronomy & Astrophysics*, 658, A183, doi: [10.1051/0004-6361/202142070](https://doi.org/10.1051/0004-6361/202142070)
- Bowler, B. P., Blunt, S. C., & Nielsen, E. L. 2020, *Astronomical Journal*, 159, 63, doi: [10.3847/1538-3881/ab5b11](https://doi.org/10.3847/1538-3881/ab5b11)
- Bowler, B. P., Kraus, A. L., Bryan, M. L., et al. 2017, *The Astronomical Journal*, 154, 165, doi: [10.3847/1538-3881/aa88bd](https://doi.org/10.3847/1538-3881/aa88bd)
- Bowler, B. P., Tran, Q. H., Zhang, Z., et al. 2023, *The Astronomical Journal*, 165, 164, doi: [10.3847/1538-3881/acbd34](https://doi.org/10.3847/1538-3881/acbd34)
- Bromley, B. C. 1992, *Publications of the Astronomical Society of the Pacific*, 104, 1049, doi: [10.1086/133089](https://doi.org/10.1086/133089)
- Bromley, B. C., Leonard, A., Quintanilla, A., et al. 2021, *The Astronomical Journal*, 162, 98, doi: [10.3847/1538-3881/ac05be](https://doi.org/10.3847/1538-3881/ac05be)
- Brott, I., & Hauschildt, P. H. 2005, in *Proc. Gaia Symp. on "The Three-Dimensional Universe with Gaia"*, Vol. 576, Obs. de Paris-Meudon (ESA SP-576), 565. [http://adsabs.harvard.edu/cgi-bin/nph-data\\_query?bibcode=2005ESASP.576..565B&link\\_type=ABSTRACT](http://adsabs.harvard.edu/cgi-bin/nph-data_query?bibcode=2005ESASP.576..565B&link_type=ABSTRACT)
- Bryan, M. L., Benneke, B., Knutson, H. A., Batygin, K., & Bowler, B. P. 2018, *Nature Astronomy*, 128, 63, doi: [10.1086/591924](https://doi.org/10.1086/591924)
- Bryan, M. L., Chiang, E., Morley, C. V., Mace, G. N., & Bowler, B. P. 2021, *The Astronomical Journal*, 162, 217, doi: [10.3847/1538-3881/ac1bb1](https://doi.org/10.3847/1538-3881/ac1bb1)
- Bryan, M. L., Ginzburg, S., Chiang, E., et al. 2020, *The Astrophysical Journal*, 905, 37, doi: [10.3847/1538-4357/abc0ef](https://doi.org/10.3847/1538-4357/abc0ef)
- Bujang, M. A., & Baharum, N. 2016, *World Journal of Social Science Research*, 3, 37, doi: [10.22158/wjssr.v3n1p37](https://doi.org/10.22158/wjssr.v3n1p37)
- Caldwell, D. A., Jenkins, J. M., & Ting, E. B. 2020a, *TESS Light Curves From Full Frame Images ("TESS-SPOC")*, STScI/MAST, doi: [10.17909/T9-WPZ1-8S54](https://doi.org/10.17909/T9-WPZ1-8S54)
- Caldwell, D. A., Tenenbaum, P., Twicken, J. D., et al. 2020b, *RNAAS*, 4, 201, doi: [10.48550/arxiv.2011.05495](https://doi.org/10.48550/arxiv.2011.05495)
- Calvet, N., & Gullbring, E. 1998, *The Astrophysical Journal*, 509, 802, doi: [10.1086/306527](https://doi.org/10.1086/306527)
- Capistrant, B. K., Soares-Furtado, M., Vanderburg, A., et al. 2022, *The Astrophysical Journal Supplement Series*, 263, 14, doi: [10.3847/1538-4365/ac9125](https://doi.org/10.3847/1538-4365/ac9125)
- Catala, C., Donati, J. F., Böhm, T., Landstreet, J., & al., e. 1999, *A&A*, 345, 884
- Cheetham, A., Huélamo, N., Lacour, S., Gregorio-Monsalvo, I. d., & Tuthill, P. 2015, *Monthly Notices RAS Letters*, 450, L1, doi: [10.1093/mnrasl/slv033](https://doi.org/10.1093/mnrasl/slv033)

- Chen, C. H., & Jura, M. 2003, *ApJ*, 591, 267
- Chiang, E. I., & Goldreich, P. 1997, *Astrophysical Journal* v.490, 490, 368, doi: [10.1086/304869](https://doi.org/10.1086/304869)
- Close, L. M., Males, J. R., Follette, K. B., et al. 2014, *A&A*, astro-ph.IM, 5096
- Close, L. M., Males, J. R., Li, J., et al. 2025, *The Astronomical Journal*, 169, 35, doi: [10.3847/1538-3881/ad8648](https://doi.org/10.3847/1538-3881/ad8648)
- Cody, A. M., Tayar, J., Hillenbrand, L. A., Matthews, J. M., & Kallinger, T. 2013, *The Astronomical Journal*, 145, 79, doi: [10.1088/0004-6256/145/3/79](https://doi.org/10.1088/0004-6256/145/3/79)
- Corder, S., Eisner, J., & Sargent, A. 2005, *ApJ*, L133
- Costigan, G., Vink, J. S., Scholz, A., Ray, T., & Testi, L. 2014, *Monthly Notices of the Royal Astronomical Society*, 440, 3444, doi: [10.1093/mnras/stu529](https://doi.org/10.1093/mnras/stu529)
- Cugno, G., Quanz, S. P., Hunziker, S., et al. 2019, *Astronomy & Astrophysics*, 622, A156, doi: [10.1051/0004-6361/201834170](https://doi.org/10.1051/0004-6361/201834170)
- Cugno, G., Zhou, Y., Thanathibodee, T., et al. 2023, arXiv
- Currie, T., Marois, C., Cieza, L., et al. 2019, *A&A*, astro-ph.EP, L3, doi: [10.3847/2041-8213/ab1b42](https://doi.org/10.3847/2041-8213/ab1b42)
- Currie, T., Lawson, K., Schneider, G., et al. 2022, *Nature Astronomy*, 751, doi: [10.1038/s41550-022-01634-x](https://doi.org/10.1038/s41550-022-01634-x)
- Cushing, M. C., Marley, M. S., Saumon, D., et al. 2008, *The Astrophysical Journal*, 678, 1372, doi: [10.1086/526489](https://doi.org/10.1086/526489)
- Debes, J., Nealon, R., Alexander, R., et al. 2023, *The Astrophysical Journal*, 948, 36, doi: [10.3847/1538-4357/acbdf1](https://doi.org/10.3847/1538-4357/acbdf1)
- Demars, D., Bonnefoy, M., Dougados, C., et al. 2023, *Astronomy & Astrophysics*, 676, A123, doi: [10.1051/0004-6361/202346221](https://doi.org/10.1051/0004-6361/202346221)
- DeWarf, L. E., Sepinsky, J. F., Guinan, E. F., Ribas, I., & Nadalin, I. 2003, *The Astrophysical Journal*, 590, 357, doi: [10.1086/374979](https://doi.org/10.1086/374979)
- Dong, J., Jiang, Y.-F., & Armitage, P. J. 2021, *The Astrophysical Journal*, 921, 0, doi: [10.3847/1538-4357/ac1941](https://doi.org/10.3847/1538-4357/ac1941)
- Eggen, O. J. 1975, *PASP*, 87, 37
- Eisner, J. A., Lane, B. F., Hillenbrand, L. A., Akeson, R. L., & Sargent, A. I. 2004, *ApJ*, 613, 1049
- Fendt, C. 2003, *A&A*, 411, 623, doi: [10.1051/0004-6361:20034154](https://doi.org/10.1051/0004-6361:20034154)
- Finkenzeller, U. 1983, *A&A*, 124, 157
- Fitton, S., Tofflemire, B. M., & Kraus, A. L. 2022, *RNAAS*, 6, 18
- Fitzpatrick, E. L. 1999, *The Publications of the Astronomical Society of the Pacific*, 111, 63, doi: [10.1086/316293](https://doi.org/10.1086/316293)
- Flasseur, O., The, S., Denis, L., Thiebaut, E., & Langlois, M. 2021, *Astronomy & Astrophysics*, 651, A62, doi: [10.1051/0004-6361/202038957](https://doi.org/10.1051/0004-6361/202038957)
- Follette, K. B., Rameau, J., Dong, R., et al. 2017, *The Astronomical Journal*, 153, 0, doi: [10.3847/1538-3881/aa6d85](https://doi.org/10.3847/1538-3881/aa6d85)
- Follette, K. B., Close, L. M., Males, J. R., et al. 2023, *The Astronomical Journal*, 165, 225, doi: [10.3847/1538-3881/acc183](https://doi.org/10.3847/1538-3881/acc183)
- Fortney, J. J., Marley, M. S., Saumon, D., & Lodders, K. 2008, *The Astrophysical Journal*, 683, 1104, doi: [10.1086/589942](https://doi.org/10.1086/589942)
- Fukagawa, M., Hayashi, M., Tamura, M., et al. 2004, *The Astrophysical Journal*, 605, L53, doi: [10.1086/420699](https://doi.org/10.1086/420699)
- Fung, J., Zhu, Z., & Chiang, E. 2019, *The Astrophysical Journal*, 887, 152, doi: [10.3847/1538-4357/ab53da](https://doi.org/10.3847/1538-4357/ab53da)
- Gaia Collaboration, Vallenari, A., Brown, A. G. A., & Prusti, T. 2022, arxiv:2208.00211
- Gaia Collaboration, Prusti, T., Bruijine, J. H. J. d., et al. 2016, *A&A*, 595, A1, doi: [10.1051/0004-6361/201629272](https://doi.org/10.1051/0004-6361/201629272)
- Gaidos, E. J. 1994, *Icarus*, 109, 382, doi: [10.1006/icar.1994.1101](https://doi.org/10.1006/icar.1994.1101)
- Garcia Lopez, R., Natta, A., Testi, L., & Habart, E. 2006, *Astronomy & Astrophysics*, 459, 837, doi: [10.1051/0004-6361:20065575](https://doi.org/10.1051/0004-6361:20065575)
- Grady, C. A., Woodgate, B., Bruhweiler, F. C., et al. 1999, *ApJ*, L151
- Gratton, R., Ligi, R., Sissa, E., et al. 2019, *Astronomy & Astrophysics*, 623, A140, doi: [10.1051/0004-6361/201834760](https://doi.org/10.1051/0004-6361/201834760)
- Haffert, S. Y., Bohn, A. J., Boer, J., et al. 2019, *Nature Astronomy*, 3, 749, doi: [10.1038/s41550-019-0780-5](https://doi.org/10.1038/s41550-019-0780-5)
- Harrington, D. M., & Kuhn, J. R. 2007, *The Astrophysical Journal*, 667, L89, doi: [10.1086/521999](https://doi.org/10.1086/521999)
- Hartmann, L., Herczeg, G., & Calvet, N. 2016, *Annual Review of Astronomy and Astrophysics*, 54, 135, doi: [10.1146/annurev-astro-081915-023347](https://doi.org/10.1146/annurev-astro-081915-023347)
- Hashimoto, J., Aoyama, Y., Konishi, M., et al. 2020, *The Astronomical Journal*, 159, 0, doi: [10.3847/1538-3881/ab811e](https://doi.org/10.3847/1538-3881/ab811e)
- Hashimoto, J., Tamura, M., Muto, T., et al. 2011, *The Astrophysical Journal*, 729, L17, doi: [10.1088/2041-8205/729/2/117](https://doi.org/10.1088/2041-8205/729/2/117)
- Herbig, G. H. 1960, *ApJS*, 4, 337
- . 1962, *AdA&A*, 1, 47
- Huélamo, N., Lacour, S., Tuthill, P., et al. 2011, *A&A*, 528, L7, doi: [10.1051/0004-6361/201016395](https://doi.org/10.1051/0004-6361/201016395)
- Huélamo, N., Chauvin, G., Mendigutía, I., et al. 2022, *Astronomy & Astrophysics*, 668, A138, doi: [10.1051/0004-6361/202243918](https://doi.org/10.1051/0004-6361/202243918)



- Ingleby, L., Calvet, N., Herczeg, G., et al. 2013, *ApJ*, 767, 112, doi: [10.1088/0004-637x/767/2/112](https://doi.org/10.1088/0004-637x/767/2/112)
- Isella, A., Benisty, M., Teague, R., et al. 2019, *The Astrophysical Journal Letters*, 879, 0 , doi: [10.3847/2041-8213/ab2a12](https://doi.org/10.3847/2041-8213/ab2a12)
- Jenkins, J. M., Twicken, J. D., McCauliff, S., et al. 2016, *Proc. SPIE*, 9913, 99133E, doi: [10.1117/12.2233418](https://doi.org/10.1117/12.2233418)
- Jorquera, S., Bonnefoy, M., Betti, S., et al. 2022, *The Astrophysical Journal*, 926, 0 , doi: [10.3847/1538-4357/ac4be4](https://doi.org/10.3847/1538-4357/ac4be4)
- Juillard, S., Christiaens, V., & Absil, O. 2023, *Astronomy & Astrophysics*, 679, A52, doi: [10.1051/0004-6361/202347259](https://doi.org/10.1051/0004-6361/202347259)
- Keppler, M., Benisty, M., Müller, A., et al. 2018, *Astronomy and Astrophysics*, 617, A44, doi: [10.1051/0004-6361/201832957](https://doi.org/10.1051/0004-6361/201832957)
- Kluska, J., Berger, J.-P., Malbet, F., et al. 2020, *Astronomy & Astrophysics*, 636, A116, doi: [10.1051/0004-6361/201833774](https://doi.org/10.1051/0004-6361/201833774)
- Kraus, A. L., & Ireland, M. J. 2012, *The Astrophysical Journal*, 745, 5, doi: [10.1088/0004-637x/745/1/5](https://doi.org/10.1088/0004-637x/745/1/5)
- Law, C. J., Booth, A. S., & Öberg, K. I. 2023, *The Astrophysical Journal Letters*, 952, L19, doi: [10.3847/2041-8213/acdfd0](https://doi.org/10.3847/2041-8213/acdfd0)
- Liffman, K., Bryan, G., Hutchison, M., & Maddison, S. T. 2020, *Monthly Notices of the Royal Astronomical Society*, 493, 4022, doi: [10.1093/mnras/staa402](https://doi.org/10.1093/mnras/staa402)
- Lightkurve Collaboration, Miranda, C. V. d., Hedges, C., et al. 2018, *Lightkurve: Kepler and TESS time series analysis in Python*, *Astrophysics Source Code Library*, ascl:1812.013
- Liu, M. C. 2004, *Science*, 305, 1442 , doi: [10.1126/science.1102929](https://doi.org/10.1126/science.1102929)
- Lubow, S. H., & Martin, R. G. 2012, *The Astrophysical Journal*, 749, L37, doi: [10.1088/2041-8205/749/2/L37](https://doi.org/10.1088/2041-8205/749/2/L37)
- Males, J. R., Close, L. M., Guyon, O., et al. 2020, *Adaptive Optics Systems VII*, 11448, 114484L, doi: [10.1117/12.2561682](https://doi.org/10.1117/12.2561682)
- Manara, C. F., Testi, L., Herczeg, G. J., et al. 2017, *Astronomy & Astrophysics*, 604, A127, doi: [10.1051/0004-6361/201630147](https://doi.org/10.1051/0004-6361/201630147)
- Mannings, V., & Sargent, A. I. 1997, *The Astrophysical Journal*, 490, 792, doi: [10.1086/304897](https://doi.org/10.1086/304897)
- Marleau, G.-D., Aoyama, Y., Hashimoto, J., & Zhou, Y. 2024, *The Astrophysical Journal*, 964, 70, doi: [10.3847/1538-4357/ad1ee9](https://doi.org/10.3847/1538-4357/ad1ee9)
- Marleau, G.-D., Aoyama, Y., Kuiper, R., et al. 2022, *A&A*, 657, 38, doi: [10.1051/0004-6361/202037494](https://doi.org/10.1051/0004-6361/202037494)
- Marois, C., Lafrenière, D., Doyon, R., Macintosh, B., & Nadeau, D. 2006, *The Astrophysical Journal*, 641, 556, doi: [10.1086/500401](https://doi.org/10.1086/500401)
- Marsh, K. A., Cleve, J. E. V., Mahoney, M. J., Hayward, T. L., & Houck, J. R. 1995, *ApJ*, 777
- Martinez, R. A., & Kraus, A. L. 2022, *The Astronomical Journal*, 163, 36, doi: [10.3847/1538-3881/ac3745](https://doi.org/10.3847/1538-3881/ac3745)
- MAST Team. 2021, *TESS Light Curves - All Sectors*, STScI/MAST, doi: [10.17909/T9-NMC8-F686](https://doi.org/10.17909/T9-NMC8-F686)
- Mazoyer, J., Arriaga, P., Hom, J., et al. 2020, *Ground-based and Airborne Instrumentation for Astronomy VIII*, 251, doi: [10.1117/12.2560091](https://doi.org/10.1117/12.2560091)
- McJunkin, M., France, K., Schneider, P. C., et al. 2014, *The Astrophysical Journal*, 780, 150, doi: [10.1088/0004-637x/780/2/150](https://doi.org/10.1088/0004-637x/780/2/150)
- Mendigutía, I., Calvet, N., Montesinos, B., et al. 2011, *Astronomy & Astrophysics*, 535, A99, doi: [10.1051/0004-6361/201117444](https://doi.org/10.1051/0004-6361/201117444)
- Millan-Gabet, R., Schloerb, F. P., & Traub, W. A. 2001, *ApJ*, 546, 358
- Millan-Gabet, R., Monnier, J. D., Berger, J.-P., et al. 2006, *ApJ*, 645, L77
- Mouillet, D., Larwood, J. D., Papaloizou, J. C. B., & Lagrange, A.-M. 1997, *Monthly Notices of the Royal Astronomical Society*, 292, 896, doi: [10.1093/mnras/292.4.896](https://doi.org/10.1093/mnras/292.4.896)
- Muzerolle, J., Flaherty, K., Balog, Z., et al. 2009, *The Astrophysical Journal*, 704, L15 , doi: [10.1088/0004-637x/704/1/L15](https://doi.org/10.1088/0004-637x/704/1/L15)
- Müller, A., Keppler, M., Henning, T., et al. 2018, *A&A*, 617, L2 , doi: [10.1051/0004-6361/201833584](https://doi.org/10.1051/0004-6361/201833584)
- Nealon, R., Pinte, C., Alexander, R., Mentiplay, D., & Dipierro, G. 2019, *Monthly Notices of the Royal Astronomical Society*, 484, 4951, doi: [10.1093/mnras/stz346](https://doi.org/10.1093/mnras/stz346)
- Norris, B., Schworer, G., Tuthill, P., et al. 2015, *Monthly Notices of the Royal Astronomical Society*, 447, 2894 , doi: [10.1093/mnras/stu2529](https://doi.org/10.1093/mnras/stu2529)
- Olofsson, J., Benisty, M., Augereau, J.-C., et al. 2011, *A&A*, 1 , doi: [10.1051/0004-6361/201016074](https://doi.org/10.1051/0004-6361/201016074)
- Oppenheimer, B. R., Brenner, D., Hinkley, S., et al. 2008, *The Astrophysical Journal*, 679, 1574, doi: [10.1086/587778](https://doi.org/10.1086/587778)
- Ortiz, J. L., Sugerma, B. E. K., Cueva, I. d. l., et al. 2010, *Astronomy & Astrophysics*, 519, A7, doi: [10.1051/0004-6361/201014438](https://doi.org/10.1051/0004-6361/201014438)
- Pairet, B., Cantalloube, F., & Jacques, L. 2021, *Monthly Notices of the Royal Astronomical Society*, 503, 3724, doi: [10.1093/mnras/stab607](https://doi.org/10.1093/mnras/stab607)

- Palma-Bifani, P., Chauvin, G., Bonnefoy, M., et al. 2022, arXiv
- Pearce, L. A., Kraus, A. L., Dupuy, T. J., et al. 2019, *The Astronomical Journal*, 157, 71, doi: [10.3847/1538-3881/aafacb](https://doi.org/10.3847/1538-3881/aafacb)
- Perrin, M. D., Schneider, G., Duchene, G., et al. 2009, *The Astrophysical Journal*, 707, L132 , doi: [10.1088/0004-637x/707/2/1132](https://doi.org/10.1088/0004-637x/707/2/1132)
- Phillips, M. W., Tremblin, P., Baraffe, I., et al. 2020, *Astronomy & Astrophysics*, 637, A38, doi: [10.1051/0004-6361/201937381](https://doi.org/10.1051/0004-6361/201937381)
- Pinilla, P., Benisty, M., Boer, J. d., et al. 2018, *The Astrophysical Journal*, 868, 85, doi: [10.3847/1538-4357/aae824](https://doi.org/10.3847/1538-4357/aae824)
- Piétu, V., Guilloteau, S., & Dutrey, A. 2005, *Astronomy & Astrophysics*, 443, 945, doi: [10.1051/0004-6361:20042050](https://doi.org/10.1051/0004-6361:20042050)
- Plunkett, C., Follette, K. B., Marleau, G.-D., & Nielsen, E. 2024, arXiv, doi: [10.48550/arxiv.2408.01491](https://doi.org/10.48550/arxiv.2408.01491)
- Prusti, T., & Mitsukevich, A. S. 1994, in *ASP Conf. Ser.* 62, *The Nature and Evolutionary Status of Herbig Ae/Be Stars*, ed. P. S. The et al. (San Francisco, CA: ASP), 257
- Quillen, A. C., & Trilling, D. E. 1998, *The Astrophysical Journal*, 508, 707, doi: [10.1086/306421](https://doi.org/10.1086/306421)
- Rameau, J., Follette, K. B., Pueyo, L., et al. 2017, *The Astronomical Journal*, 153, 244, doi: [10.3847/1538-3881/aa6cae](https://doi.org/10.3847/1538-3881/aa6cae)
- Rest, A., Sinnott, B., & Welch, D. L. 2012, *Publications of the Astronomical Society of Australia*, 29, 466, doi: [10.1071/as11058](https://doi.org/10.1071/as11058)
- Ricker, G. R., Winn, J. N., Vanderspek, R., et al. 2014, *A&A*, astro-ph.EP
- Rivière-Marichalar, P., Fuente, A., Gal, R. L., et al. 2020, *Astronomy & Astrophysics*, 642, A32, doi: [10.1051/0004-6361/202038549](https://doi.org/10.1051/0004-6361/202038549)
- Rivière-Marichalar, P., Macías, E., Baruteau, C., et al. 2023, arXiv
- Rodríguez, L. F., Zapata, L. A., Dzib, S. A., et al. 2014, *The Astrophysical Journal Letters*, 793, L21, doi: [10.1088/2041-8205/793/1/L21](https://doi.org/10.1088/2041-8205/793/1/L21)
- Rota, A. A., Meijerhof, J. D., Marel, N. v. d., et al. 2024, arxiv:2401.05798v1
- Sallum, S., Eisner, J., Skemer, A., & Murray-Clay, R. 2023, *The Astrophysical Journal*, 953, 55, doi: [10.3847/1538-4357/ace16c](https://doi.org/10.3847/1538-4357/ace16c)
- Sallum, S., Follette, K. B., Eisner, J. A., et al. 2015a, *Nature*, 527, 342 , doi: [10.1038/nature15761](https://doi.org/10.1038/nature15761)
- Sallum, S., Eisner, J. A., Close, L. M., et al. 2015b, *ApJ*, 801, 85, doi: [10.1088/0004-637x/801/2/85](https://doi.org/10.1088/0004-637x/801/2/85)
- Salyk, C., Herczeg, G. J., Brown, J. M., et al. 2013, *The Astrophysical Journal*, 769, 21, doi: [10.1088/0004-637x/769/1/21](https://doi.org/10.1088/0004-637x/769/1/21)
- Salyk, C., Pontoppidan, K., Corder, S., et al. 2014, *ApJ*, 792, 68, doi: [10.1088/0004-637x/792/1/68](https://doi.org/10.1088/0004-637x/792/1/68)
- Sanford, R. F., & Merrill, P. W. 1958, *PASP*, 602
- Sanghi, A., Zhou, Y., & Bowler, B. P. 2022, *The Astronomical Journal*, 163, 0 , doi: [10.3847/1538-3881/ac477e](https://doi.org/10.3847/1538-3881/ac477e)
- Schmid, H. M., Bazzon, A., Roelfsema, R., et al. 2018, *Astronomy & Astrophysics*, 619, A9, doi: [10.1051/0004-6361/201833620](https://doi.org/10.1051/0004-6361/201833620)
- Shenavrin, V. I., Grinin, V. P., Baluev, R. V., & Demidova, T. V. 2019, *Astronomy Reports*, 63, 1035, doi: [10.1134/s1063772919120060](https://doi.org/10.1134/s1063772919120060)
- Shenavrin, V. I., Grinin, V. P., Rostopchina-Shakhovskaja, A. N., Demidova, T. V., & Shakhovskoi, D. N. 2012, *Astronomy Reports*, 56, 379, doi: [10.1134/s1063772912040063](https://doi.org/10.1134/s1063772912040063)
- Sitko, M. L., Carpenter, W. J., Kimes, R. L., et al. 2008, *ApJ*, 678, 1070
- Smith, J. C., Stumpe, M. C., Cleve, J. E. V., et al. 2012, *Publications of the Astronomical Society of the Pacific*, 124, 1000, doi: [10.1086/667697](https://doi.org/10.1086/667697)
- Soubiran, C., Champion, J.-F. L., Brouillet, N., & Chemin, L. 2016, *Astronomy & Astrophysics*, 591, A118, doi: [10.1051/0004-6361/201628497](https://doi.org/10.1051/0004-6361/201628497)
- Soummer, R., Pueyo, L., & Larkin, J. 2012, *The Astrophysical Journal*, 755, L28, doi: [10.1088/2041-8205/755/2/L28](https://doi.org/10.1088/2041-8205/755/2/L28)
- Sparks, W. B., White, R. L., Lupu, R. E., & Ford, H. C. 2018, *The Astrophysical Journal*, 854, 134, doi: [10.3847/1538-4357/aaa549](https://doi.org/10.3847/1538-4357/aaa549)
- Speedie, J., Dong, R., Hall, C., et al. 2024, *Nature*, 633, 58, doi: [10.1038/s41586-024-07877-0](https://doi.org/10.1038/s41586-024-07877-0)
- Stassun, K. G., & Torres, G. 2021, *The Astrophysical Journal Letters*, 907, 0 , doi: [10.3847/2041-8213/abdaad](https://doi.org/10.3847/2041-8213/abdaad)
- Stassun, K. G., Oelkers, R. J., Paegert, M., et al. 2019, *The Astronomical Journal*, 158, 138, doi: [10.3847/1538-3881/ab3467](https://doi.org/10.3847/1538-3881/ab3467)
- Stelzer, B., Scholz, A., & Jayawardhana, R. 2007, *The Astrophysical Journal*, 671, 842, doi: [10.1086/521431](https://doi.org/10.1086/521431)
- Stumpe, M. C., Smith, J. C., Catanzarite, J. H., et al. 2014, *Publications of the Astronomical Society of the Pacific*, 126, 100, doi: [10.1086/674989](https://doi.org/10.1086/674989)
- Stumpe, M. C., Smith, J. C., Cleve, J. E. V., et al. 2012, *Publications of the Astronomical Society of the Pacific*, 124, 985, doi: [10.1086/667698](https://doi.org/10.1086/667698)

- Szulágyi, J., Binkert, F., & Surville, C. 2022, *The Astrophysical Journal*, 924, 1, doi: [10.3847/1538-4357/ac32d1](https://doi.org/10.3847/1538-4357/ac32d1)
- Tang, H. 2012, 1
- Tang, Y. W., Guilloteau, S., Piétu, V., et al. 2012, *Astronomy and Astrophysics*, 547, A84, doi: [10.1051/0004-6361/201219414](https://doi.org/10.1051/0004-6361/201219414)
- Tang, Y.-W., Guilloteau, S., Dutrey, A., et al. 2017, *The Astrophysical Journal*, 840, 0, doi: [10.3847/1538-4357/aa6af7](https://doi.org/10.3847/1538-4357/aa6af7)
- Tanigawa, T., Ohtsuki, K., & Machida, M. N. 2012, *ApJ*, 747, 47, doi: [10.1088/0004-637x/747/1/47](https://doi.org/10.1088/0004-637x/747/1/47)
- Tannirkulam, A., Monnier, J. D., Millan-Gabet, R., et al. 2008a, *ApJ*, 677, L51
- Tannirkulam, A., Monnier, J. D., Harries, T. J., et al. 2008b, *The Astrophysical Journal*, 689, 513, doi: [10.1086/592346](https://doi.org/10.1086/592346)
- Taylor, A. G., & Adams, F. C. 2024, *Icarus*, 415, 116044, doi: [10.1016/j.icarus.2024.116044](https://doi.org/10.1016/j.icarus.2024.116044)
- Thalmann, C., Janson, M., Garufi, A., et al. 2016, *The Astrophysical Journal Letters*, 828, L17, doi: [10.3847/2041-8205/828/2/117](https://doi.org/10.3847/2041-8205/828/2/117)
- Thanathibodee, T., Calvet, N., Bae, J., Muzerolle, J., & Hernández, R. F. 2019, *The Astrophysical Journal*, 885, 0, doi: [10.3847/1538-4357/ab44c1](https://doi.org/10.3847/1538-4357/ab44c1)
- Turner, N. J., Carballido, A., & Sano, T. 2010, *The Astrophysical Journal*, 708, 188, doi: [10.1088/0004-637x/708/1/188](https://doi.org/10.1088/0004-637x/708/1/188)
- Villenave, M., Stapelfeldt, K. R., Duchêne, G., et al. 2024, *The Astrophysical Journal*, 961, 95, doi: [10.3847/1538-4357/ad0c4b](https://doi.org/10.3847/1538-4357/ad0c4b)
- Wagner, K., Follette, K. B., Close, L. M., et al. 2018, *The Astrophysical Journal Letters*, 863, L8, doi: [10.3847/2041-8213/aad695](https://doi.org/10.3847/2041-8213/aad695)
- Wang, J., Ruffio, J.-B., Rosa, R. J. D., et al. 2015, *Astrophysics Source Code Library*, ascl:1506.001
- Ward, W. R., & Canup, R. M. 2010, *The Astronomical Journal*, 140, 1168, doi: [10.1088/0004-6256/140/5/1168](https://doi.org/10.1088/0004-6256/140/5/1168)
- Wichittanakom, C., Oudmaijer, R. D., Fairlamb, J. R., et al. 2020, *Monthly Notices of the Royal Astronomical Society*, 493, 234, doi: [10.1093/mnras/staa169](https://doi.org/10.1093/mnras/staa169)
- Wisniewski, J. P., Clampin, M., Grady, C. A., et al. 2008, *ApJ*, 682, 548
- Wolff, S. G., Menard, F., Caceres, C., et al. 2017, *The Astronomical Journal*, 154, 0, doi: [10.3847/1538-3881/aa74cd](https://doi.org/10.3847/1538-3881/aa74cd)
- Wu, Y.-L., Cheng, Y.-C., Huang, L.-C., et al. 2023, *The Astronomical Journal*, 166, 143, doi: [10.3847/1538-3881/acedb0](https://doi.org/10.3847/1538-3881/acedb0)
- Wu, Y.-L., Sheehan, P. D., Males, J. R., et al. 2017, *ApJ*, 836, 1, doi: [10.3847/1538-4357/aa5b96](https://doi.org/10.3847/1538-4357/aa5b96)
- Wu, Y.-L., Bowler, B. P., Sheehan, P. D., et al. 2022, *The Astrophysical Journal Letters*, 930, L3, doi: [10.3847/2041-8213/ac6420](https://doi.org/10.3847/2041-8213/ac6420)
- Xie, C., Haffert, S. Y., Boer, J. d., et al. 2020, *Astronomy & Astrophysics*, 644, A149, doi: [10.1051/0004-6361/202038242](https://doi.org/10.1051/0004-6361/202038242)
- Xuan, J. W., Hsu, C.-C., Finnerty, L., et al. 2024, *The Astrophysical Journal*, 970, 71, doi: [10.3847/1538-4357/ad4796](https://doi.org/10.3847/1538-4357/ad4796)
- Yoshida, T. C., Nomura, H., Law, C. J., et al. 2024, *The Astrophysical Journal Letters*, 971, L15, doi: [10.3847/2041-8213/ad654c](https://doi.org/10.3847/2041-8213/ad654c)
- Zhou, Y., Herczeg, G. J., Kraus, A. L., Metchev, S., & Cruz, K. L. 2014, *The Astrophysical Journal*, 783, L17, doi: [10.1088/2041-8205/783/1/117](https://doi.org/10.1088/2041-8205/783/1/117)
- Zhou, Y., Bowler, B. P., Wagner, K. R., et al. 2021, *The Astronomical Journal*, 161, 244, doi: [10.3847/1538-3881/abeb7a](https://doi.org/10.3847/1538-3881/abeb7a)
- Zhou, Y., Sanghi, A., Bowler, B. P., et al. 2022, *The Astrophysical Journal Letters*, 934, 0, doi: [10.3847/2041-8213/ac7fef](https://doi.org/10.3847/2041-8213/ac7fef)
- Zhou, Y., Bowler, B. P., Yang, H., et al. 2023, *The Astronomical Journal*, 166, 220, doi: [10.3847/1538-3881/acf9ec](https://doi.org/10.3847/1538-3881/acf9ec)
- Zhu, Z. 2015, *ApJ*, 799, 16, doi: [10.1088/0004-637x/799/1/16](https://doi.org/10.1088/0004-637x/799/1/16)
- . 2018, *Monthly Notices of the Royal Astronomical Society*, 483, 4221, doi: [10.1093/mnras/sty3358](https://doi.org/10.1093/mnras/sty3358)
- Zhu, Z., Ju, W., & Stone, J. M. 2016, *The Astrophysical Journal*, 832, 1, doi: [10.3847/0004-637x/832/2/193](https://doi.org/10.3847/0004-637x/832/2/193)
- Zurlo, A., Cugno, G., Montesinos, M., et al. 2020, *Astronomy & Astrophysics*, 633, A119, doi: [10.1051/0004-6361/201936891](https://doi.org/10.1051/0004-6361/201936891)